Vision Research 72 (2012) 14–33

Contents lists available at SciVerse ScienceDirect

Vision Research

journal homepage: www.elsevier.com/locate/visres

Standardized *F*1 – A consistent measure of strength of modulation of visual responses to sine-wave drifting gratings

M. Wypych [a], C. Wang [b], A. Nagy [c], G. Benedek [c], B. Dreher [b], W.J. Waleszczyk [a,*]

[a] Nencki Institute of Experimental Biology, Pasteur 3 St., 02-093 Warsaw, Poland
[b] School of Medical Sciences & Bosch Institute, The University of Sydney, NSW 2065, Australia
[c] The University of Szeged, Dóm tér 10, 6720 Szeged, Hungary

ARTICLE INFO

Article history:
Received 17 August 2011
Received in revised form 3 September 2012
Available online 18 September 2012

Keywords:
Gratings induced modulation
Modulation index
Primary visual cortex
Caudate nucleus
Superior colliculus
Suprageniculate nucleus

ABSTRACT

The magnitude of spike-responses of neurons in the mammalian visual system to sine-wave luminance-contrast-modulated drifting gratings is modulated by the temporal frequency of the stimulation. However, there are serious problems with consistency and reliability of the traditionally used methods of assessment of strength of such modulation. Here we propose an intuitive and simple tool for assessment of the strength of modulations in the form of standardized *F*1 index, *zF*1. We define *zF*1 as the ratio of the difference between the *F*1 (component of amplitude spectrum of the spike-response at temporal frequency of stimulation) and the mean value of spectrum amplitudes to standard deviation along all frequencies in the spectrum. In order to assess the validity of this measure, we have: (1) examined behavior of *zF*1 using spike-responses to optimized drifting gratings of single neurons recorded from four 'visual' structures (area V1 of primary visual cortex, superior colliculus, suprageniculate nucleus and caudate nucleus) in the brain of commonly used visual mammal – domestic cat; (2) compared the behavior of *zF*1 with that of classical statistics commonly employed in the analysis of steady-state responses; (3) tested the *zF*1 index on simulated spike-trains generated with threshold-linear model. Our analyses indicate that *zF*1 is resistant to distortions due to the low spike count in responses and therefore can be particularly useful in the case of recordings from neurons with low firing rates and/or low net mean responses. While most V1 and a half of caudate neurons exhibit high *zF*1 indices, the majorities of collicular and suprageniculate neurons exhibit low *zF*1 indices. We conclude that despite the general shortcomings of measuring strength of modulation inherent in the linear system approach, *zF*1 can serve as a sensitive and easy to interpret tool for detection of modulation and assessment of its strength in responses of visual neurons.

1. Introduction

The firing rates of neurons in the mammalian visual system are modulated by temporal frequency of luminance-contrast-modulated sine-wave gratings drifting through their receptive fields. The strength of modulation varies substantially from neuron to neuron and depends on stimulus parameters (e.g. spatial and temporal frequencies of gratings). In the case of primary visual cortex (striate cortex, cytoarchitectonic area 17, area V1) neurons these modulations have been quite extensively investigated for several decades (for fairly recent review see Mechler & Ringach, 2002). Oscillations in the magnitude of spike-responses in step with temporal frequency of drifting gratings were also observed in the case of single neurons recorded from cat's insular cortex (Hicks, Benedek, & Thurlow, 1988), the dorsolateral segment of caudate nucleus (CN, Nagy et al., 2008) or subcortical components of the ascending tectofugal visual system such as superficial layers of the superior colliculus (SC, Waleszczyk et al., 2007), lateral posterior-pulvinar complex (Casanova, Freeman, & Nordmann, 1989) or the suprageniculate nucleus of the posterior thalamus (Sg, Paróczy et al., 2006).

There is a fundamental need for establishment of consistent and reliable method of quantification of the strength of modulation of the magnitude of spike-responses. The primary choice, that is usually considered, is the modulation index (*MI*) defined as the ratio of the magnitude of response (number of action potentials – spikes) at the fundamental temporal frequency of the stimulus (*F*1 component) to the magnitude of averaged net response or, assuming very low background ('spontaneous') activity, over the magnitude of the averaged response (*F*0), in other words, the *F*1 to *F*0 ratio. *MI* was originally introduced by Movshon, Thompson, and Tolhurst (1978a, 1978b) when assessing the degree of linearity in spatial

* Corresponding author. Address: Laboratory of Visual System, Department of Neurophysiology, Nencki Institute of Experimental Biology, Pasteur 3 St., 02-093 Warsaw, Poland. Fax: +48 22 8225342.
E-mail address: w.waleszczyk@nencki.gov.pl (W.J. Waleszczyk).

0042-6989/$ - see front matter © 2012 Elsevier Ltd. All rights reserved.
http://dx.doi.org/10.1016/j.visres.2012.09.004

summation within the receptive fields of single neurons in the primary visual cortex of anaesthetized domestic cats. Indeed, in the case of most neurons in area V1, the *MI* appears to be a quite reliable and convenient measure of the strength of modulation of response to optimized gratings and provides additional information about response linearity and structure of the receptive fields (e.g. Skottun et al., 1991).

However, the *MI* is not an appropriate measure in conditions where the responses of neurons are characterized by a combination of high background ('spontaneous') spike-activity and/or weak responses (low spike-response rate). This includes most neurons recorded from the subcortical components of the ascending tectofugal system. Moreover, a substantial proportion of area V1 neurons, is characterized by a combination of low background spike-activity and weak responses, and this results in a substantial increase ('boosting') of the *MI* value. This in turn, as pointed out by Crowder and his colleagues (2007), might lead to 'misidentification' of cortical cells as simple (that is, cells with presumptively high degree of linearity in spatial summation within their receptive fields) rather than complex (cells presumed to have a low degree of linearity in spatial summation within their receptive fields). Furthermore, *MI* yields low values not only when there is no modulation in the spike-rate response, but also when modulations are relatively weak yet visible in peristimulus time histograms (PSTHs) of spike-responses and indicated as a clear peak at stimulus frequency in the frequency spectrum computed from the PSTHs. When recording neuronal activity from subcortical components of the ascending tectofugal system we noticed that visual stimulation causing a small change in the cell's mean firing rate might result in substantial changes of the *MI* value, irrespective of the actual degree of gratings-induced modulation of neuronal discharges. Theoretically, net response, and thus *MI*, can also be negative due to suppression of background neuronal activity by visual stimulation or when the stimulus influences only the temporal pattern of spiking activity, leaving the level of firing rate comparable to that of background activity (Wypych et al., 2009b). Thus, we argue that it is very worthwhile to establish a more reliable measure of modulation of spiking activity in the responses of visual neurons. The development of such a measure is especially critical in the case of multi-channel recordings with automated data analyses where on-line visual assessment of temporal modulation in PSTHs and the peaks in Fourier spectra for individual cells becomes impossible.

In the present study we propose a new index (standardized *F*1 value or *zF*1) for detection of modulations in spiking activity and determining strength of the modulations. The *zF*1 index is defined as the ratio of a difference between the *F*1 component of the response and the mean value of the amplitude spectrum to the standard deviation (*SD*) of amplitude values along all frequencies in the spectrum. Here, we describe a method for computing *zF*1, provide arguments for the validity of this new measure and compare its behavior with established methods used for the analysis of steady-state responses in electro- and magneto-encephalography (Ahmar, Wang, & Simon, 2005; Mitra & Pesaran, 1999; Picton et al., 2001, 1987; Victor & Mast, 1991). We also consider different methods of frequency spectrum estimation. In the analyses we used spike-responses to drifting gratings of single neurons from four brain structures of anaesthetized and pharmacologically immobilized domestic cat: A17, SC, Sg and CN, and also simulated spike-trains. Our study indicates that *zF*1, which is straightforward to calculate and interpret, is a suitable tool for detection and quantitative assessment of oscillatory form of modulations of neuronal spiking activity even in the case of recordings with low firing rates and/or low net mean magnitude of responses.

Preliminary analyses were presented in form of published abstracts (Wypych et al., 2010, 2009a).

2. Experimental methods

Experimental data were collected in two laboratories from two different continents. Although some aspects of the data analysis were published earlier (Bardy et al., 2006; Nagy et al., 2008; Paróczy et al., 2006; Waleszczyk et al., 2007), the data were extensively re-analyzed for the purpose of the present study. Single neuron recordings from area 17 were conducted at the University of Sydney, Australia (Bardy et al., 2006) while single unit recordings from the SC, Sg and CN were conducted at the University of Szeged, Hungary (Nagy et al., 2008; Paróczy et al., 2006; Waleszczyk et al., 2007).

2.1. Area 17 experiments

2.1.1. Animal preparation, surgical procedures and anesthesia

Experimental procedures and husbandry for the recordings from cat area 17 followed the guidelines of the Australian Code of Practice for the Care and Use of Animals for Scientific Purposes and were approved by the Animal Care Ethics Committees at the University of Sydney.

To reduce the possibility of brain oedema, on the day preceding the experiment the animals were given dexamethasone phosphate (0.3 mg/kg, i.m; Dexapent). The animals were initially anesthetized with a gaseous mixture of 2.5–5.0% halothane in N_2O/O_2 (67%/33%). Tracheal and cephalic vein cannulations were performed to allow artificial ventilation and infusion of paralyzing drugs.

During the recording session anesthesia was maintained with a gaseous mixture of N_2O/O_2 (67%/33%) and halothane (0.4–0.7%). Antibiotic (amoxycillin trihydrate, 75 mg), dexamethasone phosphate (3 mg) and atropine sulfate (0.3 mg) were injected i.m. daily. Immobility was induced with i.v. injection of 80 mg gallamine triethiodide in 2 ml of sodium lactate (Hartmann's) solution and maintained with continuous injection of gallamine triethiodide (10 mg/kg/h i.v.) in a mixture of equal parts of 5% dextrose solution and Hartmann's solution. Residual eye movements were additionally minimized by bilateral sympathectomy (Rodieck et al., 1967).

Throughout the experiment the animals were artificially ventilated via a tracheal cannula with peak expired CO_2 maintained at 3.7–4.0% by adjusting stroke volume and/or rate of the pulmonary pump. The body temperature, monitored by subscapular probe, was maintained automatically at about 37.5 °C with a servo-controlled heating blanket. The heart rate was monitored continuously and maintained in the range 180–240 beats/min (depending on animal weight) by adjusting the halothane level in the gaseous mixture. The electroencephalogram (EEG) recorded with a metal screw touching the dura over the frontal cortex (contralateral to A17 recorded from) was also monitored continuously. A 'deep sleep' state characterized by δ waves (~0.5–4.0 Hz) in the EEG was maintained by adjusting the halothane when necessary.

The corneas were protected with zero-power, air-permeable contact lenses. Pupils were dilated, accommodation blocked and nictitating membranes retracted with application of an aqueous solution of 1% atropine sulfate and 0.1% phenylephrine hydrochloride (Isopto-Frin, Alcon). Artificial pupils (3 mm in diameter) and corrective lenses appropriate to focus the eyes on a tangent screen located 57 cm away, were positioned in front of the eyes. The optic disc of each eye was back projected daily on the tangent screen using a fiber optic light source and the position of the *area centralis* was plotted directly and/or by reference to the optic disc (cf. Bishop, Kozak, & Vakkur, 1962; Sanderson & Sherman, 1971).

2.1.2. Extracellular recording of neuronal activity

The craniotomy was performed over area 17 (HC coordinates: L 0–5, P 0–10). A stainless steel microelectrode of high impedance

(7–12 MΩ: FHC, USA) was advanced vertically into area 17 using a hydraulic micromanipulator (David Kopf Instruments). Action potentials from single neurons were recorded extracellularly, conventionally amplified and monitored both visually and acoustically. Triggering was continuously monitored on an oscilloscope. Triggered standard pulses were fed into a computer for data collection. Spike times were stored with 0.1 ms resolution.

2.1.3. Visual stimulation

First, the excitatory discharge fields of recorded neurons were plotted separately for each eye (with the other eye covered) using elongated light bars (generated by a hand-held ophthalmoscope) and hand-held elongated dark bars of optimal orientation. The ocular dominance class was determined by listening to the audio-monitor and subjective assessment of the relative magnitude of responses to optimally oriented stimuli presented separately via each eye (e.g. Hubel & Wiesel, 1962; cf. Burke et al., 1992). For binocular cells, the excitatory discharge fields (the 'minimum response fields' of Barlow, Blakemore, & Pettigrew, 1967) were plotted separately for each eye. The cells were qualitatively identified as: (1) simple if they had spatially distinct 'ON' and 'OFF' discharge regions and/or spatially separate discharge regions for the light and dark bars in their receptive fields, or (2) complex if they had spatially overlapping 'ON' and 'OFF' discharge regions and/or spatially overlapping light bar and dark bar discharge regions in their receptive fields (Hubel & Wiesel, 1959, 1962; cf. Burke et al., 1992; Gilbert, 1977; Henry, 1977). For quantitative identification of cell as simple or complex the classical modulation index, *MI* (Movshon, Thompson, & Tolhurst, 1978a, 1978b) was used. Quantitative identification of cell as a simple ($MI > 1$) or complex ($MI < 1$; De Valois, Albrecht, & Thorell, 1982; see for review Skottun et al., 1991) and assessment of other features of receptive fields were conducted using stimuli presented separately via each eye. Description of the *MI* value is presented in the Data analysis section.

Luminance-contrast-modulated sine-wave drifting gratings were generated by a visual stimulation system, VSG 5, (Cambridge Research System, UK) and presented on a CRT monitor (BARCO, Belgium) placed 57 cm from the cat's eyes. To ensure that the gratings indeed had a sinusoidal luminance profile, linearizing of the luminance of the display on the CRT monitor based on the Look-Up-Tables was conducted every 2–3 months.

After mapping the excitatory discharge fields with hand-held stimuli response tunings of the cell in respect to the different parameters (orientation, direction, spatial and temporal frequencies) of high (80–100%) contrast sine-wave modulated drifting gratings were quantitatively determined. Each stimulus parameter was optimized before subsequent tuning measure. Following estimation of contrast tuning we assessed the spatial extent of the classical receptive field or summation receptive field, that is, the size of the patch of optimized (optimal orientation, direction, spatial and temporal frequencies) high (but not saturating) contrast grating which produced the strongest spike-response. Recordings with each stimulation parameters were repeated in pseudo-random order three (for optimization of stimulation parameters) to six times (for assessment of spatial extent of the classical receptive field) with each recording usually lasting 3 or 4 s. The background activity was defined as the activity during presentation of gray screen (0% contrast stimulation).

2.2. SC, Sg and CN experiments

2.2.1. Animal preparation, surgical procedures and anesthesia

Cats of either sex weighing from 2.4 to 3.5 kg were used in these experiments. All experimental procedures were carried out to minimize the number of the animals and followed the European Communities Council Directive of 24 November 1986 (S6 609 EEC) and National Institutes of Health guidelines for the care and use of animals for experimental procedures. The experimental protocol had been approved by the Ethical Committee for Animal Research of the University of Szeged. The animals were initially anesthetized with ketamine hydrochloride (30 mg/kg i.m., Calypsol). To reduce salivation and bronchial secretion a subcutaneous injection of 0.2 ml 0.1% atropine sulfate was administered preoperatively. The trachea and the femoral vein were cannulated and the animals were placed in a stereotaxic headholder. All wounds and pressure points were routinely infiltrated with local anesthetic (procaine hydrochloride, 1%). Throughout the surgery the anesthesia was continued with halothane (1.6%, Fluothane) in air. The animals were immobilized with gallamine triethiodide (20 mg/kg). During recording sessions gallamine triethiodide (8 mg/kg/h), glucose (10 mg/kg/h) and dextran (50 mg/kg/h) in Ringer lactate solution was infused at a rate of 4 ml/h. Atropine sulfate (1–2 drops, 0.1%) and phenylephrine hydrochloride (1–2 drops, 10%) were applied locally to respectively dilate the pupils and block accommodation, and retract the nictitating membranes. The ipsilateral eye was occluded during the visual stimulation. During the recording sessions, anesthesia was maintained with a gaseous mixture of air and halothane (about 0.8%). The end-tidal concentration of halothane, MAC values and peak CO_2 concentrations were monitored with a capnometer (Capnomac Ultima, Datex-Ohmeda, Inc.). The heart rate and brain activity (EKG and EEG) were also monitored continuously. During the length of the anesthesia the EEG displayed a slow wave sleep. The peak expired CO_2 was kept in the range 3.8 to 4.2%. The body temperature was maintained at approx. 37.5 °C using a warm-water heating blanket with thermostat.

2.2.2. Extracellular recording of neuronal activity

The skull was opened to allow a vertical approach to the desired structure. Vertical penetrations were performed between the Horsley-Clarke co-ordinates A 12–16, L 4–6.5, H 2–9 to record neuronal activity from CN; A 1–3, L 1–3, H 3.5–5 to record neuronal activity from superficial layers of SC and A 4.5–6.5, L 4–6.5, H 1–3 to record neuronal activity from Sg. Electrophysiological recordings of single units were carried out extracellularly via tungsten microelectrodes (AM System Inc., USA; 2–4 MΩ). Single-cell discrimination was performed with a spike-separator system (SPS-8701, Australia), after high-pass filtering of the recorded signal (>500 Hz). At the end of the experiments, the animals were deeply anesthetized with pentobarbital (200 mg/kg i.v.) and perfused transcardially with 4% paraformaldehyde solution. The brains were removed and cut into coronal sections of 50 μm, which were subsequently stained with Neutral Red. Recording sites were localized on the basis of the marks of the electrode penetrations. Only neurons recorded from either CN, superficial retino-recipient layers of the SC or the Sg were used for analyses.

2.2.3. Visual stimulation

Spatio-temporal frequency characteristics of each unit were tested with drifting sine-wave gratings displayed on a CRT monitor (refresh rate: 80 Hz) positioned at a distance of 42.5 cm away from the cat's eye. To obtain the most preferred direction of the movement for each cell, gratings were moved in eight different directions (0–315° at 45° increments). The preferred direction was then used for determination of the spatio-temporal frequency characteristic of the tested cell. The contrast of the grating was held constant at 96%. The mean luminance of the screen was 23 cd/m^2. Stimuli were presented in a circular aperture with a diameter of 30 deg, centered on either center of the contralateral receptive field in the case of recording from SC neurons or the *area centralis* in the case of recording from CN and Sg. The spatio-temporal frequency response profiles of CN, SC and Sg cells

were assessed by using 24–93 spatio-temporal frequency combinations of drifting gratings. The tested spatial frequencies ranged from 0.025 to 0.95 cycles/deg (c/deg), while the temporal frequencies varied from 0.07 to 37.24 cycles/s (Hz). Each spatio-temporal frequency combination was presented at least 12 times in series in pseudorandom sequence with other seven spatio-temporal combinations. The presentation of the single trial overall lasted 2 s. During the first 1 s, the grating remained stationary, and was then drifted for another 1 s. The inter-stimulus interval was 0.5 s, while blank screen was shown. PSTHs were constructed online to visualize neuronal activity. To characterize the response amplitude of the CN, SC, Sg neurons the net discharge rate was used. The net discharge rate was calculated as the difference between the mean firing rates of the cell obtained during stimulus movement and the 200 ms long period preceding the onset of movement (prestimulus period; the first 800 ms of the neuronal responses to stationary stimulus was truncated, to avoid the effect of the onset of the grating). In the case of the clear changes in neuronal activity during recording not related to stimulation by drifting gratings, i.e. when the mean 'spontaneous' (background) spike activity of the cell for any series varied more than two standard errors of the means (SEM) from the background activity measured for any other series, the cell was excluded from later analysis.

3. Data analysis

Off-line data analyses were performed using MATLAB® (MathWorks, Inc.).

Amplitude spectra of response histograms were computed with a fast Fourier transform (*FFT*) algorithm. Data were not treated with any window before computing Fourier spectra (Bach & Meigen, 1999). In addition to amplitude spectra obtained by *FFT* we used two other methods of power spectrum estimation: Thomson's multitaper method (MTM, Thomson, 1982) and Welch's approach. Although Welch's method consists of computing spectra with the use of *FFT*, the computation is made from short, overlapping, segments of the signal. The obtained periodogram is then time-averaged and provides the estimation of the power spectrum. The spectra were computed with 'pwelch' Matlab function with default parameters (signals were divided into eight equal segments with 50% overlap, Hamming window was applied to each segment, before computation of *FFT*). MTM approach consists of computation of multiple, independent spectrum estimations from single trial, which are then averaged. Each independent estimation is obtained by computing of *FFT* from the signal treated with a special window. All the windows are orthogonal and taken from prolate spheroidal wave functions (Thomson, 1982). Unless stated differently, MTM was computed with 'pmtm' Matlab function, with default value of the NW parameter equal 2, resulting in 2NW-1 = 3 tapers. Both Welch and MTM approaches resulted in smoother spectra estimations than those obtained by *FFT*.

*F*0 (or mean activity, in spikes/s) values reported here are the firing rates averaged over the time of stimulus presentation in single trial or, depending on the test, averaged over all trials with given stimulus parameters. The *F*1 values reported here are the magnitudes of the first component (at stimulus temporal frequency) of the frequency spectra. In the case of recordings from subcortical structures, where visual stimulation lasted for 1 s only data obtained during stimulation with gratings drifting at temporal frequencies above 1 Hz were taken into account.

To identify and assess strength of modulations in the responses by the stimulus in form of luminance-modulated sine-wave moving gratings few different measures, representing two different approaches, were used. Consistency in phase of Fourier function component at stimulus frequency was assessed by Rayleigh's phase coherence test (RPC, Mardia, 1972; Picton et al., 1987; Ahmar, Wang, & Simon, 2005) or tests which take into account both phase and amplitude values of response: Hotelling T^2 test (Picton et al., 1987, 2001) or T^2 circular statistics (Victor & Mast, 1991). Other methods: *F*-test for hidden periodicity (FHP, Ahmar, Wang, & Simon, 2005; Picton et al., 2001) and Thomson's multitaper *F*-test (Mitra & Pesaran, 1999; Thomson, 1982) base on the comparison of magnitude of response component in the frequency spectra at frequency of stimulation, *F*1, to measurement at other frequencies in the spectra which are treated as a background or noise.

3.1. Standardized F1

In statistical analyses the standardized value is defined as a ratio of the value of variable above the population mean and the standard deviation (e.g. Siegel, 1956), or following Wikipedia, the quantity /z/ represents the distance between the raw score and the population mean in units of the standard deviation. Such standardization of data is widely used and commonly referred to as '*z*-score'. Regardless of the shape of the distribution, it transforms the data set to have mean value of zero and standard deviation equals unity.

In the present study we introduce the standardized *F*1 value, *zF*1, as a measure of modulation strength. Standardized *F*1 is defined here as the ratio of a difference between the *F*1 component of response and the mean value of amplitude spectrum to standard deviation of amplitude values along all frequencies in the spectrum (see Fig. 1):

$$zF1 = \frac{F1 - mean(FFT)}{SD(FFT)}, \quad (1)$$

where *zF*1 – standardized *F*1 value, *F*1 – amplitude component at temporal frequency of stimulation, *mean*(*FFT*) – mean amplitude of the spectrum over the range of frequencies from 1/*T* to *fpsth*/2 or Nyquist frequency, *SD*(*FFT*) – standard deviation of amplitudes in the frequency spectrum (over all frequencies from 1/*T* to *fpsth*/2) (see Fig. 1); *T* is the duration of recording of single response in seconds and *fpsth* = 1/*bs* where *bs* is bin size of PSTH in seconds.

As a result of such standardization, *zF*1 is essentially resistant to the magnitude of neural response and does not depend on the background ('spontaneous') spike activity. As a ratio of two quantities of the same units of measurement, *zF*1 is a dimensionless measure.

*zF*1 value were computed for each repetition and then averaged over trials of the same parameters of stimulation. To avoid division by equal zero standard deviation of Fourier spectrum, trials with one spike or no spike were excluded from the analyses. When the *F*1 value exceeded the mean amplitude of the spectrum by at least one *SD*(*FFT*) (*zF*1 > 1), indicating a peak in the spectrum (e.g. Figs. 1 and 2A), the response was considered to be modulated by temporal frequency of the grating, otherwise it was considered as unmodulated (*zF*1 < 1; e.g. Fig. 2B). In analyses of PSTHs we used 10 ms bins. Details of other data analyses will be presented together with description of the corresponding results.

3.2. Rayleigh's phase coherence (RPC)

The phase coherence (*R*) for *M* stimulus repetitions was calculated using the following formula:

$$R = 1/M\sqrt{\left(\sum \cos\Theta_i\right)^2 + \left(\sum \sin\Theta_i\right)^2},$$

where θ_i is the phase obtained from *FFT* at stimulus temporal frequency for *i*th stimulus presentation (trial).

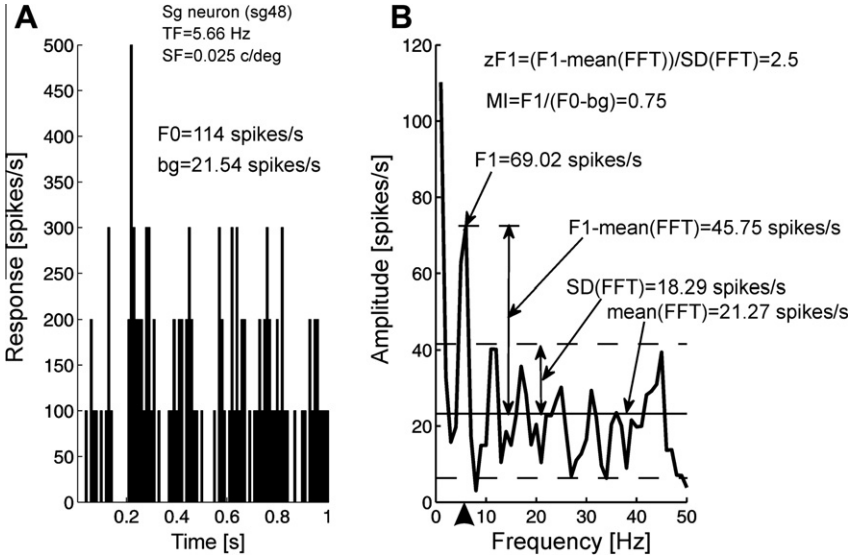

Fig. 1. Calculation of standardized *F*1 (*zF*1 index). (A) Peristimulus time histogram (PSTH) of the response of a supragenicular nucleus neuron to a single stimulus presentation. The stimulus was a luminance-modulated sine-wave drifting grating with spatial and temporal frequencies of 0.025 c/deg and 5.66 Hz, respectively. Bin size of PSTH – 10 ms. *F*0 is defined as the mean firing rate of the response averaged over the time of single stimulus presentation and can be estimated directly from the PSTH or from its amplitude spectrum, *bg* refers to background activity. (B) Amplitude spectrum computed from the PSTH shown in A. *F*1 (indicated by one of the arrows) is defined as the amplitude of response component at the stimulus temporal frequency (indicated by arrowhead at the abscissa). Continuous straight line depicts mean value of the amplitude spectrum, *mean*(*FFT*), dashed lines indicate ± standard deviation from the mean of the amplitude spectrum, *SD*(*FFT*). *zF*1 is defined as the ratio of the difference between *F*1 and *mean*(*FFT*) to *SD*(*FFT*) (Eq. (1)). Value of *zF*1 > 1 denotes temporal frequency modulation of the response. Modulation index (*MI*) is defined as the ratio of *F*1 to the net response (*F*0–*bg*).

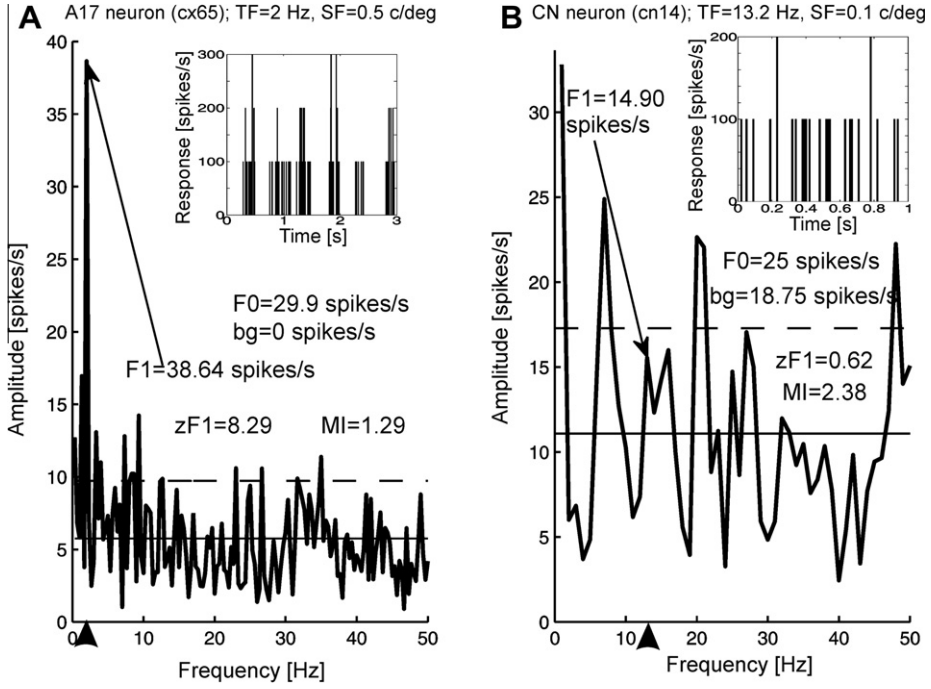

Fig. 2. Amplitude spectra computed from the corresponding PSTHs (insets) of neuronal responses to sinusoidal drifting gratings. (A) Example of an amplitude spectrum for the response of an A17 simple cell (*MI* > 1). The *zF*1 ≫ 1 indicates presence of strong modulation in the response. (B) Representative spectrum for the response of a CN neuron. The *zF*1 value (<1) indicates lack of modulation. Note, however, the high value of *MI*. PSTHs (insets) in A and B illustrate responses to single presentations of the stimulus – sine-wave drifting gratings. SF and TF indicate spatial and temporal frequencies of the stimulation, respectively. Other conventions as in Fig. 1.

The *R* varies between 0 and 1. The value closer to 1 indicates higher probability that the same phase of the response is present for every stimulus repetition. The significance of the result was assessed following Mardia (1972) or Zar (1999) using approximation:

$$P = \exp\left[\sqrt{1 + 4M + 4M^2(1 - R^2)} - (1 + 2M)\right].$$

The standard deviation of the phase (circular standard deviation or *CSD*) was calculated according Mardia (1972) in degrees:

$$CSD = 180/\pi \cdot \sqrt{-2\ln(R)},$$

where ln(*R*) is the natural logarithm of *R*.

Here the ratio of R/CSD^2 was used to asses the strength of oscillations.

3.3. T^2 statistics

The method based on T^2-statistics was firstly used by Picton and coworkers (Picton et al., 1987) for detection of oscillatory component in the recorded auditory evoked potentials. The T^2-statistics was originally proposed by Hotelling (1931) and is the multivariate analog of the square of the t value for univariate statistics (Anderson, 2003). T^2 is given by the equation:

$$T^2 = M(\mathbf{x}-\mu)'S^{-1}(\mathbf{x}-\mu),$$

where $\mathbf{x}$ is the mean vector of a sample of M, μ is the mean tested in H_0 hypothesis, and S is the sample covariance matrix. In the case of testing for modulations $\mathbf{x}$ consists of real and imaginary parts of Fourier component at stimulation temporal frequency, and μ is equal zero.

Multiplication of T^2 by $(M-k)/(k(M-1))$, where k is the number of dimensions (in our case $k = 2$) transforms the values to Fisher–Snedecor distribution with k and $M-k$ degrees of freedom, allowing to check the significance of obtained values (Picton et al., 1987).

3.4. T^2_{circ} statistics

The T^2 circular statistics (T^2_{circ}) has been introduced by Victor and Mast (1991) for analysis of steady-state visually evoked potentials as a statistics which fully utilized information about real and imaginary parts of Fourier components (for detailed formula see Victor & Mast, 1991).

Following Victor and Mast (1991), the level of significance of F-value for T^2_{circ} was taken from Fisher–Snedecor distribution for 2 and $2M-2$ degrees of freedom, where M is the number of stimulus repetitions (trials).

3.5. F-test for hidden periodicity

F-test for hidden periodicity (FHP) allows for comparison of the magnitude of response at the frequency of stimulation to averaged measures at other frequencies in the spectrum and therefore can be treated as the estimation of signal-to-noise ratio. This test, proposed by Schuster (1898) and Fisher (1929), was used successfully in the analysis of steady-state auditory responses (Picton et al., 2001) and MEG data (Ahmar, Wang, & Simon, 2005). F value was calculated according to the following formula:

$$F = KA_s^2/\Sigma A_i^2,$$

where A_s^2 is the power of the signal (sum of squares of the real and imaginary part) at the stimulus frequency, and $(1/K)\Sigma A_i^2$ is the averaged power of the signal at K frequencies excluding the frequency of stimulation. In the current paper we have considered all frequencies lower than temporal frequency of the stimulus ($K/2$) and $K/2$ frequencies higher than temporal frequency of the stimulus. The significance of F is assessed for 2 and K degrees of freedom. The F-values were then averaged over stimulus repetitions and compared to the threshold.

3.6. Thomson's multitaper F-test

Thomson's multitaper F-test (Mitra & Pesaran, 1999; Thomson, 1982) was performed using modified functions from Chronux Toolbox for Matlab (www.chronux.org; Purpura & Bokil, 2008) with parameters of time-banwidth set to 3 and number of tapers equal 5 (default values) or time-bandwidth equal 7 and number of tapers 13.

3.7. Modulation index

MI is a measure designed for assessment of linearity of responses of primary visual cortical neurons and used for classification of simple and complex cells. Cortical cells are commonly identified as simple if $MI > 1$ or as complex if $MI < 1$ (De Valois, Albrecht, & Thorell, 1982; see for review Skottun et al., 1991). *MI* is defined as a ratio of the amplitude of the response component at the stimulus temporal frequency to the average net magnitude of spike-response:

$$MI = \frac{F1}{F0 - bg},$$

where *MI* – modulation index, *F*1 – amplitude (number of spikes/s) of component of response at temporal frequency of drifting gratings, *F*0 – mean spike activity, *bg* – background ('spontaneous') spike activity.

Due to variability of responses, even for stimulation parameters evoking maximal averaged response, one can obtain for single stimulus presentations uncontrolled high or negative values of *MI*. Thus, we calculated the index using *F*1, *F*0 and *bg* values computed for single stimulus repetitions and then averaged over all trials. Trials which contained no spikes were excluded from the analyses.

*F*1 value (crucial for computation of *MI*) obtained with MTM and Welch's method would depend on arbitrary chosen parameters of the methods. Thus, here we show *MI* results obtained only with spectra calculated with use of *FFT*.

3.8. Simulations of spike-trains

With the aim to better understand the behavior of *MI* and *zF*1, the indices were computed for a range of simulated spike-trains of known structure.

We used a simple threshold-linear model (Carandini & Ferster, 2000; Mechler & Ringach, 2002; Priebe et al., 2004) which has been shown to predict well firing rates of both simple and complex cells. In the threshold-linear model, firing rate, $R(t)$ of cortical cell is proportional to membrane potential, $V_m(t)$ when it is over threshold for spike generation or zero when the membrane potential is bellow threshold:

$$R(t) = k[V_m(t) - V_{th}]^+,$$

where k indicates gain for spike generation, V_{th} corresponds to the threshold for spike generation, $[V_m(t) - V_{th}]^+ = V_m(t) - V_{th}$ for $V_m(t) > V_{th}$ and zero otherwise (Fig. 3).

In the case of response to drifting sinusoidal gratings time dependent change of membrane potential, $V(t)$, in respect to resting potential, V_{rest}, is assumed to be a sum of two components:

$$V(t) = V_1 \sin(2\pi ft) + V_0.$$

First component in the above equation represents modulated change of membrane potential with amplitude V_1 in response to drifting sinusoidal grating of temporal frequency f, and the second component, V_0, represents constant change of membrane potential (depolarization or hyperpolarization) induced by the stimulus. Thus, spiking rate is given by the formula:

$$R(t) = k[V_1 \sin(2\pi ft) + V_c]^+,$$

where $V_c = V_0 + V_{rest} - V_{th}$.

In other words, probability of generating spike is determined by the sum of two components: one modulated (given by sinusoid of certain amplitude and frequency) and the other one, unmodulated (given by constant of positive or negative value).

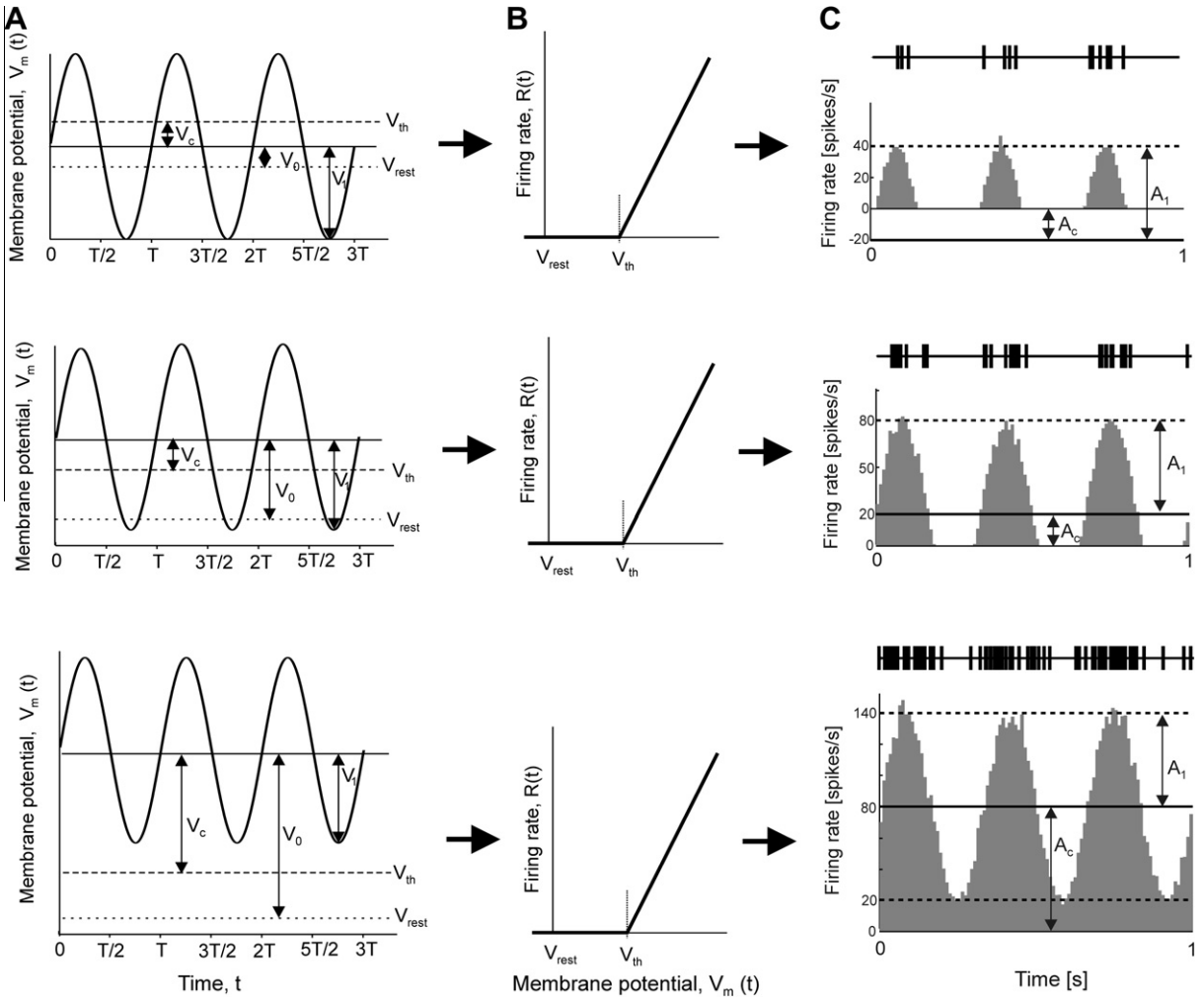

Fig. 3. Simulation of spike-trains with modulated and unmodulated components – the transformation of membrane potential (V_m) to firing rate with the threshold-linear model. (A) Examples of simulated modulations of membrane potential in response to drifting sinusoidal grating with temporal frequency $1/T$. In all three cases the magnitude of modulated component (V_1) is the same, while that of an unmodulated component (V_0) is different. V_{rest} (dotted lines) denotes resting potential, V_{th} (dashed lines) denotes threshold for spike generation, V_c – unmodulated change of membrane potential exceeding threshold. (B) The threshold-linear transformation between the membrane voltage and spike-response, $R(t)$. (C) Resulting spike-responses: representative spike-trains obtained for "single stimulus repetition" and below PSTHs obtained for 500 repeats. A_1 denotes amplitude of sinusoidal modulation in response (60 spikes/s in all examples), A_c unmodulated component of spike-response (−20, 20 and 80 spikes/s, from upper to lower panel, respectively).

In computing practice, probability of occurrence of a spike in nth 1 ms bin of simulated spike-train was given by formula:

$$P(n) = \max\{0; 0.001 * (A_1 \sin(2\pi ft) + A_c)\},$$

where n is a number of 1 ms bin, A_1 (kV_1) is the amplitude of modulated component of firing rate varying from 0 to 100 spikes/s, f is the frequency of modulation varying from 1 to 30 Hz, $t = 0.001n$ is the time (in s) corresponding to nth bin in the spike-train and A_c (kV_c) is the magnitude of unmodulated component of firing rate varying from −100 to100 spikes/s.

For each combination of parameters (A_1, A_c and f) simulation was performed 500 times to obtain reliable mean and *SD* of *MI* and *zF*1 indices. All simulations were performed for 1 s (e.g. Fig. 3) and 3 s epochs.

Each spike-train was transformed into 10 ms bin sized histogram on which Fourier transform was performed. As in the case of experimental recordings, the simulated data were not treated with any window before computing *FFT*. Then *mean*(*FFT*) and *SD*(*FFT*) values were calculated and *F*1 values corresponding to modulation frequency were extracted. Total number of spikes in the spike-train divided by the length (in seconds) of the spike-train was taken as *F*0. In all simulations background spike activity for computing *MI* was assumed to be zero. In the case of simulated data, to estimate the *SD*s of *MI* and *zF*1, the indices were computed separately for each repetition, without previous averaging of *F*1, *F*0, *mean*(*FFT*) and *SD*(*FFT*) over trials.

For $A_1 = 0$ and $A_c > 0$, spikes were uniformly randomly distributed and thus there were no modulations in the spike-trains. In such cases, random "stimulation frequency" from 1 to 30 Hz was chosen for extracting *F*1 for further analyses.

3.9. Statistical analyses

Statistical evaluation of the difference between two related sets of data was performed using non-parametric Wilcoxon matched-pairs signed-ranks test. Statistical significance of the difference was accepted if the associated probability (p) value was 0.05 or less at the two-tailed criterion. r indicating Pearson correlation coefficient is always accompanied by p-value calculated for $N - 2$ degrees of freedom, where N is the population size. The mean values in the text are accompanied by ±standard deviations (*SD*s).

4. Results

In Section 4.1 we present arguments for the validity of *zF*1 as a tool in analysis of neurophysiological data. In Section 4.2 we explore characteristics of *zF*1 on data modulated simulated spike-trains generated using threshold-linear model, and also compare behavior of *zF*1 and *MI* on simulated unmodulated data. In Section 4.3 we compare behavior of *zF*1 using the methods listed above (Sections 3.2-3.7). Since our 'subcortical data' were collected at random phase of visual stimulation, measures of steady-state responses which exploit information about phase: RPC, T^2 and T^2_{circ}, are calculated only for cortical data. We also have tested the behavior of *zF*1 using three methods of obtaining of frequency spectra. Finally, in Section 4.4, we apply *zF*1 to single-cell responses to drifting grating of optimal spatial and temporal frequencies, orientation and size recorded from four different brain structures: A17 ($N = 100$), SC ($N = 60$), Sg ($N = 105$) and CN ($N = 103$) and show relationships between *zF*1 and *F*1, *F*0 or *MI* in different parts of visual system.

4.1. Tests of validity of zF1 measure

In tests of the validity of standardized *F*1 first we considered the relation between the magnitude of response, *F*0 and two elements determining *zF*1: *mean*(*FFT*) and *SD*(*FFT*) for A17 data (Figs. 4A and B). Taking into account that the energy of the signal (PSTH) is equal to the energy of its amplitude spectrum one could expect that *mean*(*FFT*) would correlate with *F*0. Indeed, *mean*(*FFT*) and also *SD*(*FFT*) correlate well with *F*0 ($r = 0.879$, $p < 0.001$ and $r = 0.711$, $p < 0.001$, respectively). As can be seen in Fig. 4B, for strongly responding simple cells *SD*(*FFT*) is higher than that for complex cells. This is presumably due to the presence of peaks at stimulus temporal frequency and its multiples in the amplitude spectra.

The question arises whether *zF*1 should be calculated on the basis of the amplitude spectrum or on the basis of the power spectrum. Fig. 4C shows that use of amplitude spectrum and power spectrum yields very similar values of *zF*1 ($r = 0.983$, $p < 0.001$). Indeed, irrespective of the basis of the calculation (amplitude spectrum or power spectrum) 99 of the 100 responses analyzed were identified as belonging to the same category, either modulated ($zF1 > 1$) or unmodulated ($zF1 < 1$). The only exception was A17 neuron which response was classified as unmodulated when *zF*1 was computed using the amplitude spectrum and as modulated when *zF*1 was computed based on the power spectrum.

Second, we tested whether *zF*1 value depends on bin size or the sampling rate of PSTHs. Since a change of bin size can result in a change of *mean*(*FFT*) and *SD*(*FFT*) it might affect also the *zF*1 value. Fig. 4D shows *zF*1 values obtained for responses of 100 cortical cells using different bin sizes 0.1 ms, 0.5 ms, 1 ms, 5 ms and 10 ms. For cells with highly modulated responses *zF*1s calculated when data were sampled in very narrow bins were apparently greater than those calculated for 10 ms bins. However, in the weakly modulated and unmodulated cells, *zF*1 hardly depends on the bin size. The greatest differences are visible between *zF*1 values obtained for bin sizes above 1 ms, and generally, with exception to highly modulated cells, *zF*1 values at bin size of 1 ms and shorter were almost constant. In Fig. 4E, we compared *zF*1 values for A17 data calculated for 10 ms bins (PSTH sampling rate = 100 Hz) with *zF*1 calculated from PSTHs constructed for the same data using 1 ms bins (PSTH sampling rate = 1000 Hz). Although overall there was a very strong correlation between *zF*1s calculated for these two bin sizes ($r = 0.953$, $p < 0.001$), for cells with highly modulated responses there was an apparent difference in *zF*1s calculated when data were sampled in 1 ms vs. those sampled in 10 ms bins. Nevertheless, with exception to two responses (one classified as being unmodulated ($zF1 < 1$) for 10 ms bin width and as being modulated ($zF1 > 1$) for 1 ms bin width, and the other with opposite relation) 98% of responses were classified identically irrespective of the size of the bin.

The dependence of *zF*1 on the duration of recordings was also tested using responses of A17 cells. Fig. 5A reveals the differences in *zF*1 values when the calculations were made for 1 s epochs of the recorded responses vs. values based on the 3 s epochs. For this analysis responses of only 92 neurons were used. Five neurons were excluded due to the short epoch of single repetition (2 s) while three other neurons were excluded from the analysis due to their low response magnitude (lack of 1 s periods with at least two spikes). For both simple and complex cells, *zF*1 value depends strongly on the duration of the response epoch. Fig. 5A illustrates a decrease of the values calculated for 1 s epochs in comparison with those calculated for 3 s epochs ($p < 0.001$, both for simple ($N = 47$) and complex ($N = 45$) cells responses).

The observed differences for different epochs are due to different resolutions of the spectra and the fact that the same spectral energy density is to be distributed into spectra of different resolution:

$$\sum |A(\omega)|^2 = const. \tag{2}$$

For the longer recording epoch, *T*, resolution of spectrum is higher and the constant energy is divided into a higher number of frequencies ω forcing the amplitudes $A(\omega)$ to be lower. In the case of modulated responses, where part of the spectral energy of the signal is precisely accumulated at the stimulation frequency, the *F*1 value is actually not affected by varying the duration of response epoch. However, for longer epochs *mean*(*FFT*) and *SD*(*FFT*) are lower and lack of change in *F*1 results in higher values of *zF*1.

The above results imply that *zF*1 values should not be directly compared if data used for computation are based on epochs of different lengths. However, this problem can be resolved by normalization of *zF*1 with respect to recording duration. To normalize the *zF*1 to 1s lengths in the Eq. (1) (Section 3.1) one should divide *F*1 by square root of *T*, where *T* is the length of recording in seconds (see Appendix A for the derivations of the normalization). The normalization can be applied for calculation of *zF*1 irrespective of the reason of different spectra length (i.e. different length of the recordings or different bin sizes of PSTHs). Fig. 5B shows *zF*1 values calculated for 1 s epochs of the recorded responses and a 3 s epochs with the use of the proposed normalization. The coefficients of linear regression of our sample changed from (0.51,0.14) for non-normalized data (Fig. 5A, dashed line) to (0.84,0.80) after normalization (Fig. 5B, dashed line).

Here, we also consider the possible upper limit of *zF*1 for hypothetical purely sinusoidal responses assuming that the amplitude spectrum is equal zero for all frequencies except to frequency of stimulation, *F*1 (Fig. 5C). Such an upper limit does not depend on the spike count, but instead, on the length of recording or spectrum (see Appendix B for the derivations of the upper limit of *zF*1). The above proposed normalization works well also for the upper limit. After normalization to a 50 bin length of spectrum corresponding to 10 ms bin size in the PSTH of 1s length (dashed line in Fig. 5C) or to a 500 bin spectrum length corresponding to 1 ms bin size in PSTH of 1 s length (dash-dotted line in Fig. 5C), *zF*1 is virtually resistant to the length of spectrum. We did observe a small bias – a decrease of normalized *zF*1 when the spectra are composed of a very low number of bins (below 50). Analogous comparison for *MI* indicates that this index is resistant to variations in duration of recording (Fig. 5D).

4.2. Tests of behavior of zF1 index on simulated spike-trains

We tested here the behavior of *zF*1 for simulated data generated by a simple rectification model (Carandini & Ferster, 2000; Mechler

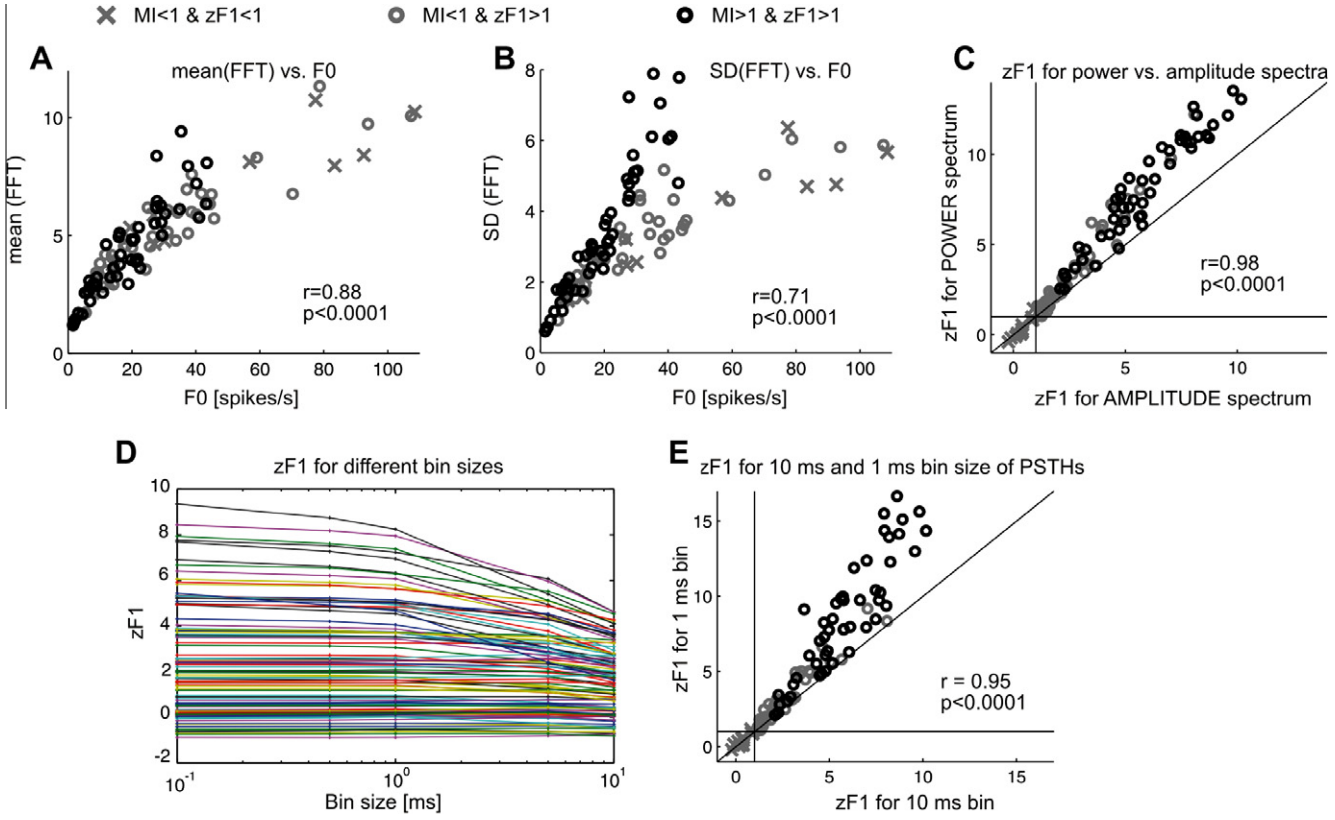

Fig. 4. Justification of the validity of *zF*1 index for A17 data obtained for optimized stimuli generating maximal net response for each of the 100 analyzed cells. (A) Relationship between mean spectrum amplitude, *mean*(*FFT*), and mean activity, *F*0. Both values are well correlated. (B) Relationship between *SD*(*FFT*) and *F*0 showing relatively good correlation ($r = 0.71$) for the whole sample. Notice, however, a difference in the relationship for cells classified as simple and those classified as complex – higher *SD*(*FFT*) for strongly responding simple cells (black circles). (C) Pairwise comparison of *zF*1 values calculated for the power spectrum and amplitude spectrum. Solid lines parallel to the abscissa and ordinate axes correspond to *zF*1 values equal 1 for the power and amplitude spectrum, respectively. Diagonal corresponds to the equality of the *zF*1 value obtained for the amplitude and power spectrum. In A, B and C bin size of PSTHs used to calculate *FFT* was 10 ms. (D) The *zF*1 values obtained for responses of 100 cortical cells for different bin sizes: 0.1 ms, 0.5 ms, 1 ms, 5 ms and 10 ms. Note that higher values of *zF*1 tend to decrease with increase in bin size. (E) Pairwise comparison of *zF*1 values calculated for PSTHs with bin sizes 1 and 10 ms. Solid lines parallel to the abscissa and ordinate correspond to *zF*1 values equal 1 (border line between modulated and unmodulated responses) for 1 and 10 ms bin sizes, respectively. Diagonal corresponds to the equal value of *zF*1 obtained for 1 and 10 ms bin size. Values of indices for both bin sizes are well correlated, however discrepancy is apparent for high values of the indices, that is, for cells with highly modulated responses. All values (*mean*(*FFT*), *SD*(*FFT*), *F*0 and *zF*1) were averaged over trials of identical stimulation parameters.

& Ringach, 2002; Priebe et al., 2004) assuming modulated and unmodulated components of stimulus-induced change in cellular membrane potential and threshold-linear transformation between membrane potential and firing rate (Fig. 3). A slight decrease of *zF*1 with an increase of modulation frequency for a range of magnitudes of unmodulated and modulated components is observed (Figs. 6A), whereas there is no dependence of *F*0 on modulation frequency (not shown). This decrease of the values of the index with the increase of modulation frequency is not present if simulated spike-trains are divided into 1 ms bins (not shown).

Fig. 6B shows the relationship between the mean spike counts in the simulated spike-trains and amplitudes of unmodulated and modulated (with temporal frequency 5 Hz) components. The average number of spikes per second (*F*0) increases with increase of the modulation amplitude, under condition when the amplitude of the modulated component is higher than that of the unmodulated component. In the case of a negative unmodulated component with the absolute value close to the amplitude of modulated component, the resulting mean spike count is low. Analogous to Fig. 6B, Fig. 6C shows dependence of *zF*1 values on the expected amplitudes of both unmodulated and modulated components – the higher the amplitude of modulated component the higher the resulting *zF*1 values. Almost everywhere, with exception of the lowest amplitudes of modulations, *zF*1 yields values higher than one, thus detecting the modulations.

Fig. 6D illustrates dependence of *zF*1 on the amplitude of modulations for set magnitudes of unmodulated component (equivalent to the horizontal sections of Fig. 6C). When the amplitude of modulated component is lower than that of unmodulated component (when the latter is positive), the index is roughly proportional to the amplitude of modulation, however, for higher amplitudes of modulations index saturates.

Fig. 6E illustrates dependence of the index on the value of the unmodulated component for set amplitudes of modulated components (equivalent to vertical sections of Fig. 6C). In particular, *zF*1 takes the maximum for a relatively low magnitude of the unmodulated component. Fig. 6F illustrates dependence of the values of the *zF*1 index for set amplitudes of modulations on the spike count (*F*0). The last panel in Fig. 6G presents two other cases. One in which amplitudes of modulated and unmodulated components are equal (equivalent to the diagonal section of upper half of Fig. 6C). This corresponds to neuronal firing, in which PSTHs have a full sinusoid shape (compare to the right panel of Fig. 3). The other case with unmodulated component equals zero (horizontal section of Fig. 6C) illustrates the behavior of *zF*1 for half-rectifying simulated model neuron. In both cases responses are strongly modulated, and both curves run close to each other. Moreover, in both cases the *zF*1 value depends on the total spike count *F*0, and tends to be lower for lower spike counts. In the case when the unmodulated component equals zero, the mean *zF*1 value exceeds

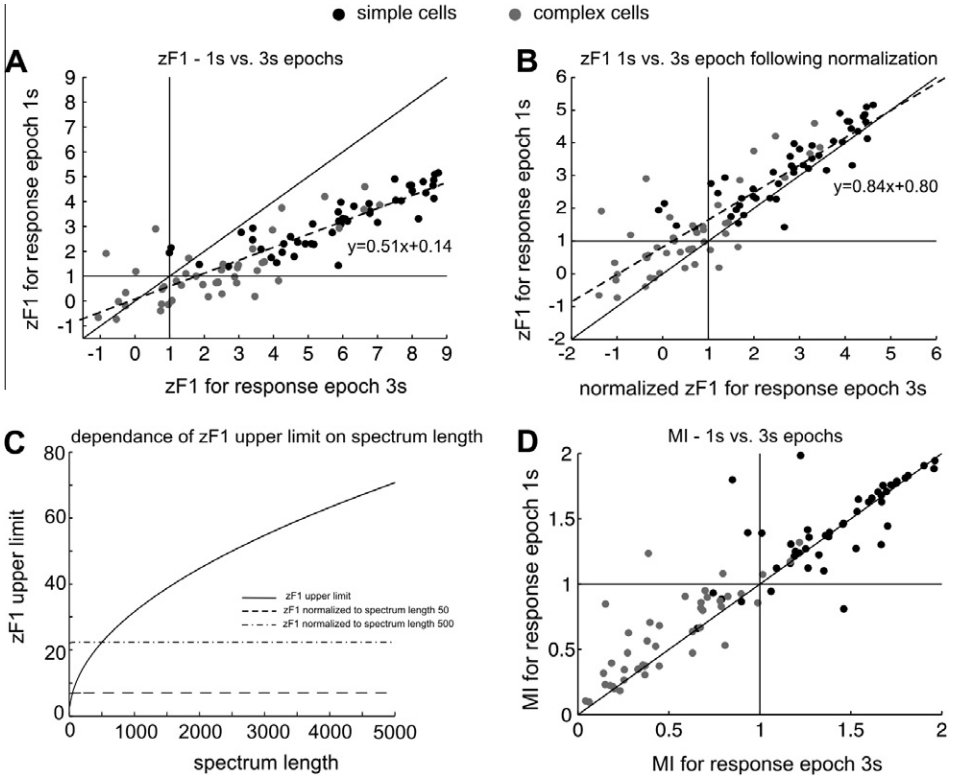

Fig. 5. Dependence of *zF*1 and *MI* values on duration of responses epochs of A17 simple and complex neurons. (A) Pairwise comparison of *zF*1 for two response epochs. The *zF*1 values calculated for 1 s epochs were significantly lower compared to 3 s epochs both for complex (Wilcoxon test, $p < 0.001$) and simple ($p < 0.001$) cells. The values for 1 s epochs are averages of values obtained for three 1 s segments of 3 s recordings. (B) Pairwise comparison of *zF*1 for two response epochs, 1 s and 3 s after normalization procedure. (C) Dependence of the upper limit of *zF*1 on the length of the spectrum. Note that after normalization to 50 bins spectrum length corresponding to 10 ms bin size in PSTH of 1 s length or to 500 bins spectrum length corresponding to 1 ms bin size in PSTH of 1 s, the upper limit of *zF*1 is virtually independent on spectrum length. Small deviation – decrease of normalized *zF*1 is apparent for very low number of bins. (D) Pairwise comparison of *MI* obtained for 3 s epoch vs. those obtained for 1 s epoch. Dashed lines in A and B represent linear regression. Cells were identified as simple or complex based on *MI* values for 3 s or 4 s recording epochs.

1 for amplitude of modulation above 3 spikes/s and saturates at a slightly higher level than for a full sinusoid. For a full sinusoid, mean *zF*1 exceeds 1 for firing rate above 5 spikes/s.

Identification of cells as simple or complex meets difficulties when one wants to use the *MI* value for categorization of cells with weak responses (low firing rate), for example when the visual stimulus is far from optimum (e.g. low contrast; Crowder et al., 2007). Due to the small value of the denominator, *MI* is boosted, what in turn, can lead to false identification of cells as simple. Although *zF*1 is not intended to classify cells into simple and complex, in the case of low net responses it may be helpful in avoiding the false identification of cells as simple.

Here, we demonstrate that the *zF*1 index is resistant to the firing rate in the case of simulated unmodulated data where spikes were randomly uniformly distributed with firing rates from 1 to 100 spikes/s. For 'responses' lasting 1 and 3 s the dependence of mean *MI* and its standard deviation (averaged over randomly chosen 'stimulation' frequencies) on spike count is shown in Fig. 7A. There is a clear increase in *MI* values with decrease of spike counts (cf. Fig. 8 in Crowder et al., 2007). The values calculated for simulations of 1 s responses are on average 1.75 ± 0.08 times higher than those of 3 s duration. Consistent with the theoretical values of *z*-score standardization, no such dependencies are found for *zF*1 (Fig. 7B), where means and standard deviations are stable; the means are close to zero and the standard deviations are close to unity. The clear increase of *MI* at low spike counts for unmodulated spike-trains indicates the need of a complementary method of detection of modulations in the responses. We believe that the *zF*1 index can serve well for this purpose.

The observed differences in values of *MI* for different lengths of response epochs are, again, due to different resolution of spectra for the data collected over different periods, and the fact, that in unmodulated data *F*1 is on the level of mean value of the spectrum, which varies with the resolution (see above consideration related to Fig. 5). No such dependence of *zF*1 on the 'response' duration was found for *zF*1 computed for unmodulated simulated data, because *mean*(*FFT*) and *SD*(*FFT*) depend on the response epoch in the same way as *F*1 (see Eq. (1)).

4.3. Comparison of zF1 with other measures for responses to drifting gratings

Here, we compare behavior of *zF*1 and other measures used to assess modulation of neural responses to drifting gratings stimulation. We use three approaches for estimation of the frequency spectra: *FFT*, MTM and Welch's method (see methods), and compare *zF*1 with five measures of strength of oscillations in steady-state responses: T^2, T^2_{circ}, RPC, FHP and Thomson's multitaper *F*-test. T^2, T^2_{circ} and R/CSD^2 are phase-sensitive measures, thus only *FFT* obtained spectra satisfy the requirements of those methods. Since our data obtained from subcortical structures were recorded during presentation of random-phase drifting gratings, we compare the above methods to *zF*1 only for A17 data.

Fig. 8 shows pairwise comparisons of *zF*1 computed for Fourier amplitude spectra and *zF*1 computed for power spectra obtained with MTM and Welch's method. There is a good correlation between *zF*1 values obtained using *FFT* and other methods of obtaining the spectra, both for Thomson's multitaper ($r = 0.80$, $p < 0.001$;

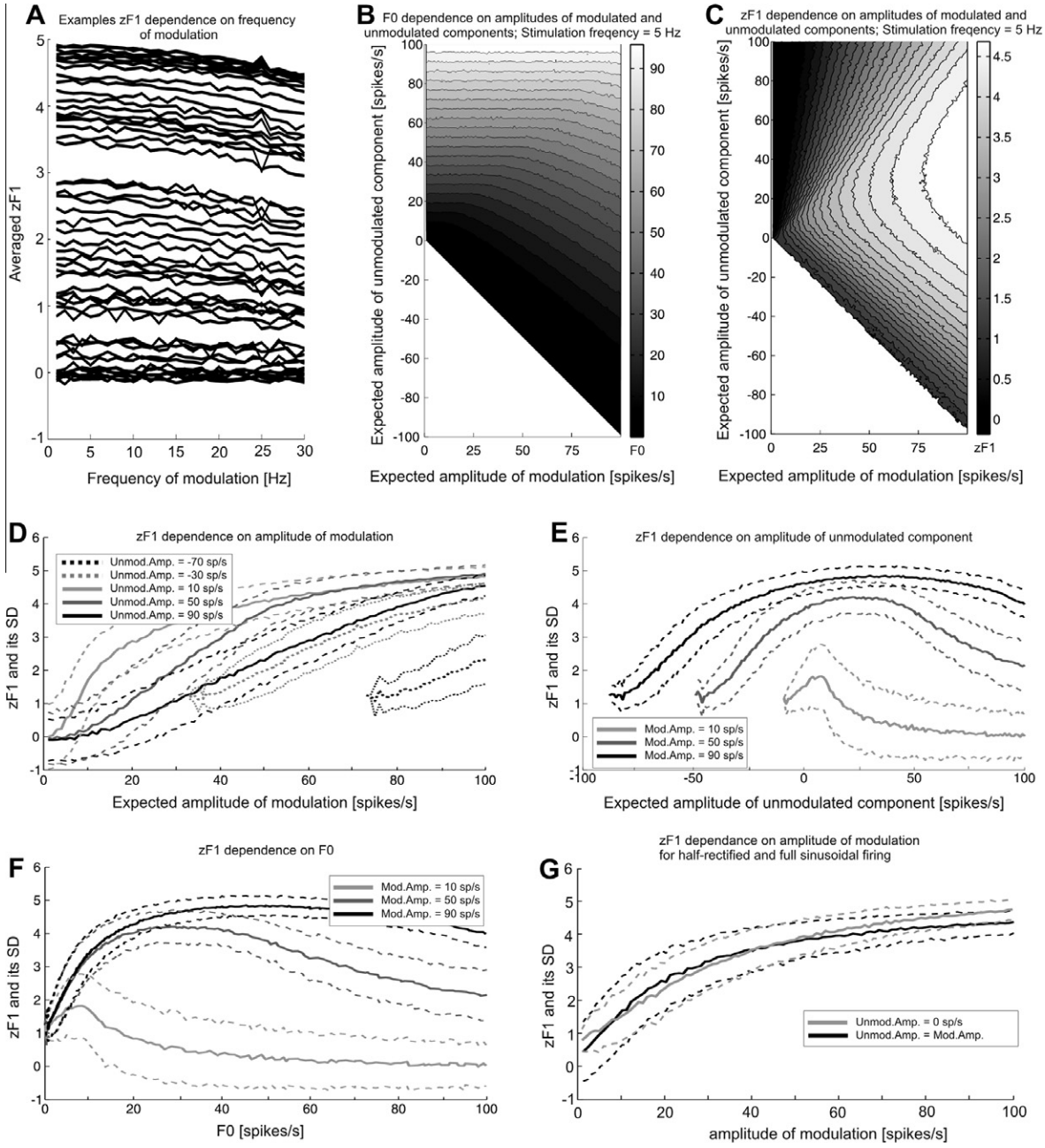

Fig. 6. Behavior of *zF*1 for simulated spike-trains with modulated and unmodulated components. The probability of spike occurrence depended on magnitudes of both unmodulated and modulated components. The modulated component varied from 1 to 100 spikes/s while the unmodulated component varied from -100 to 100 spikes/s (with 1 spike/s resolution). Modulation frequency varied from 1 to 30 Hz. Background activity was assumed to be 0 spikes/s. Data were computed for 1 s epochs. For each combination of parameters simulation was performed 500 times. (A) Examples illustrating dependence of obtained *zF*1 values on frequency of modulations for 10 ms bin width. Each curve corresponds to different combination of magnitudes of modulated (1, 5, 10, 20, 50, 100 spikes/s) and unmodulated (−1, 1, −5, +5, −10, 10, −20, 20, −50, 50, −100, and 100 spikes/s) components. There was almost no dependence on modulation frequency for 1 ms bin width (not shown), however, in the case of a bin width of 10 ms, *zF*1 takes lower values for higher frequencies of modulations. (B) Dependence of mean number of spikes in the obtained spike-trains on the amplitude of the unmodulated and modulated components. Note that modulations raise the average number of spikes when the amplitude of the modulated component is higher than that of the unmodulated component. Note also low value of *F*0 when magnitude of modulation is close to absolute value of the negative unmodulated component. The *F*0 value is represented in the intensity of gray (grayscale bar on the right). (C) Relation between *zF*1 and magnitudes of modulated and unmodulated components. Note that the index does not detect modulations (*zF*1 < 1) only when modulation amplitude is much lower than the magnitude of the unmodulated component. The *zF*1 value is coded in the intensity gray (grayscale bar on the right). (D) Dependence of *zF*1 on modulation amplitude for set values of unmodulated component. The curves correspond to horizontal sections of C with *SD* added. Note that for positive values of the unmodulated component *zF*1 is roughly linearly related to the amplitude of modulation if the amplitude is lower than the magnitude of the unmodulated component. For higher modulation amplitudes the index saturates. For negative values of the unmodulated component *zF*1 increases with growth of the modulation amplitude. (E) Dependence of *zF*1 on the value of the unmodulated component for set values of amplitudes of modulation. The curves, with SD added, correspond to vertical sections of C. The *zF*1 takes the maximum for relatively low magnitude of the unmodulated component. (F) The same data as in *E* plotted against *F*0. (G) The *zF*1 dependence on firing rate for amplitude of modulations equal mean firing rate (full sinusoid) and for amplitude of modulation equal zero (a half-rectified neuron). In the case when the unmodulated component equals zero the mean *zF*1 value exceeds 1 for amplitude of modulation above 3 spikes/s and saturates on the higher level than for a full sinusoid. For a full sinusoid the mean *zF*1 exceeds 1 for firing rate above 5 spikes/s. In B–G temporal frequency of modulation is 5 Hz.

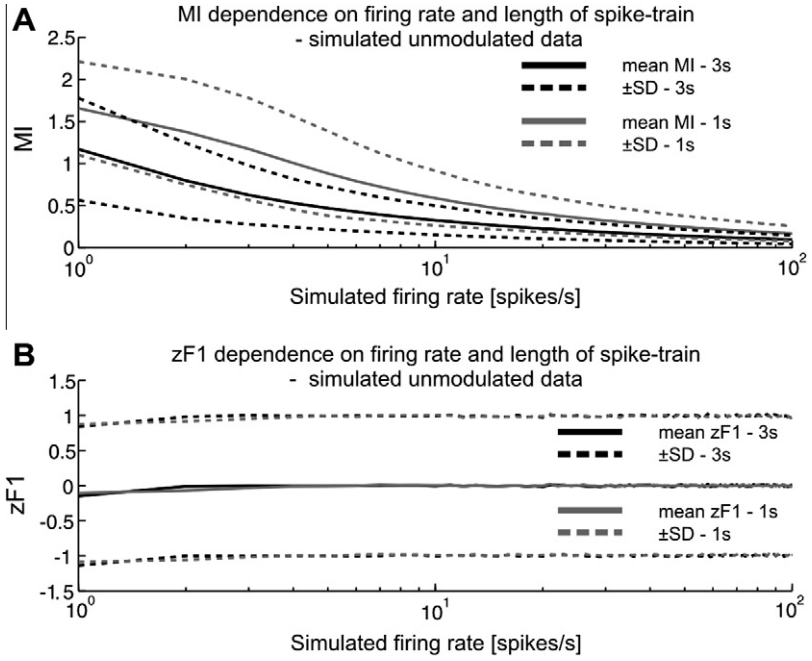

Fig. 7. Relationship between spike counts and *MI* (A) and *zF*1 (B) values obtained from simulations of unmodulated spike-trains with uniform random spike distribution over 'response' interval. Note negative correlation between the number of spikes in simulated responses and the *MI* and its standard deviation both for 1 s (gray solid and dashed line, respectively) and 3 s (black lines) 'response' epochs. No such dependence is apparent for *zF*1. For 1 and 3 s periods mean *zF*1 values are stable, close to zero and, consistent with the *z*-score standardization theory, their standard deviations are close to unity. Note the increase of *MI* values for shorter 'response' epochs. Spike-trains were simulated for various probabilities of spike count, from 1 to 100 spikes/s, uniformly and randomly distributed and put into 10 ms bin sized histograms. Fourier transform was computed and *MI* and *zF*1 values were calculated for randomly chosen 'stimulation frequency' from 1 to 30 Hz. Since no dependence on stimulation frequency was found for *MI* or for *zF*1, plots were obtained by averaging results for all frequencies. Background activity for computation of *MI* was assumed to be 0 spikes/s.

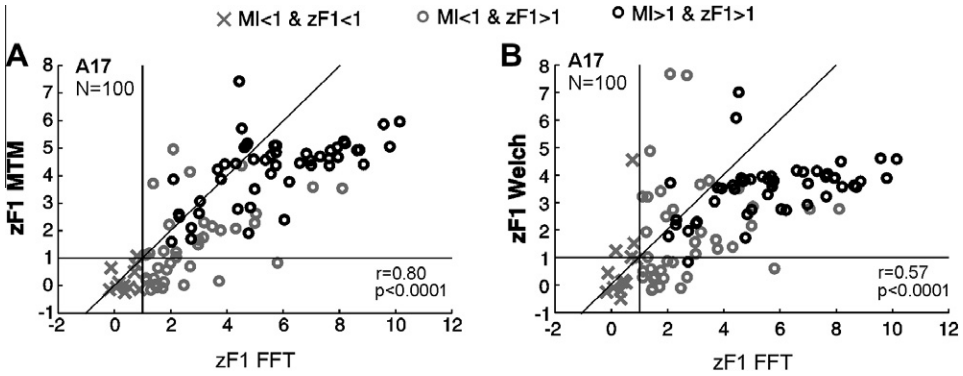

Fig. 8. Pairwise comparison of *zF*1 values obtained for calculation of amplitude spectra of neuronal responses to optimal stimulus recorded from A17 with the use of *FFT* (abscissa) vs. *zF*1 values obtained when power spectra for the same spike trains were calculated with Thomson's multitaper (MTM) (A) or Welch's (B) approaches. In all cases, bin size of PSTH which was a subject of spectral analysis, was uniformly 10 ms. Multitaper function (pmtm.m) was used with the parameter nw = 2 resulting in three tapers. Power spectrum was computed with Welch method (pwelch.m) using eight segments with 50% overlap of segments. Note the strong correlation between *zF*1 values obtained using *FFT* and other methods. Notice also that *zF*1 values for spectra obtained with MTM and Welch's approaches for strongly modulated responses tend to be lower than obtained with *FFT*.

Fig. 8A) and Welch's approach ($r = 0.57$, $p < 0.001$; Fig. 8B). As can be seen in both panels of Fig. 8, most points is located below the diagonals indicating a higher sensitivity of *zF*1 computed using conventional Fourier spectra. This is most likely due to the fact, that both Welch and multitaper approaches result in smoother spectra than those obtained with *FFT* and both lead to broadening of possible modulation peaks. This in turn affects standard deviations of the spectra and leads to lower *zF*1 values. In the case of both methods the broadness of the peak depends on the values of arbitrarily set parameters.

Fig. 9 shows pairwise comparison of *zF*1 with FHP (A), T^2 (B), T^2_{circ} (C) and R/CSD^2 (D) and Thomson's multitaper *F*-test (E) for cortical recordings. The *zF*1 indicated 87% of neurons (87/100) as cells with modulation in the responses (*zF*1 > 1). All measures correlated well with *zF*1. The best correlation was obtained between values of *zF*1 and FHP ($r = 0.70$, $p < 0.001$; Fig. 9A), that is, the other index based on the comparison of response amplitude estimation at stimulus frequency to amplitudes at other frequencies in the spectrum. The level of significance of the *F*-value depended on the number of frequencies used for the "control" level (see methods) thus was different for different neurons and varied between 3.23 and 19, and in sum it was reached for 46% of A17 neurons (45/98). The correlation of *zF*1 with the measures which take into account similarity between both amplitudes and phases across trials was weaker. Fig. 9B presents correlation plot of *zF*1 and F values for T^2 test ($r = 0.33$, $p < 0.001$). The level of significance depended on

number of stimulus repetitions (see methods) and varied between 4.74 and 199. Overall, 60% (59/98) of neurons were considered to exhibit significant modulations of responses to drifting gratings. Fig. 9C shows analogous data for T^2_{circ} statistics ($r = 0.57$, $p < 0.001$). The level of significance (see methods) varied between 3.63 and 19, and overall 69% (68/98) of neurons were considered as significantly modulated.

The ratio of Rayleigh's phase coherence and circular variance (see methods) is compared with $zF1$ in Fig. 9D. The correlation took value of $r = 0.55$, $p < 0.001$. According to the test, modulations were significant in 57 (out of 100) neurons.

We have also tested Thomson's multitaper F-test especially designed for multitaper method of spectrum estimation. The test was calculated with Chronux Toolbox with multitaper parameters of bandwidth equal 7 and number of tapers equal 13. The obtained F-values (averaged over repetitions; Fig. 9E) also correlated well with $zF1$ ($r = 0.51$, $p < 0.001$). Only in 15% (15/100) of neurons, the modulations were significant according to the test. For parameters used, the level of significance for F-value varied between 25.28 and 29.83. Lower values of parameters, e.g. default (bandwidth 3, number of tapers 5), resulted in similar $zF1$ values, but due to smaller number of tapers thresholds for F-value significance were much higher and resulted in non or very few significant results (not shown). On the other hand, higher values of parameters resulted in broader modulation peaks in the spectra.

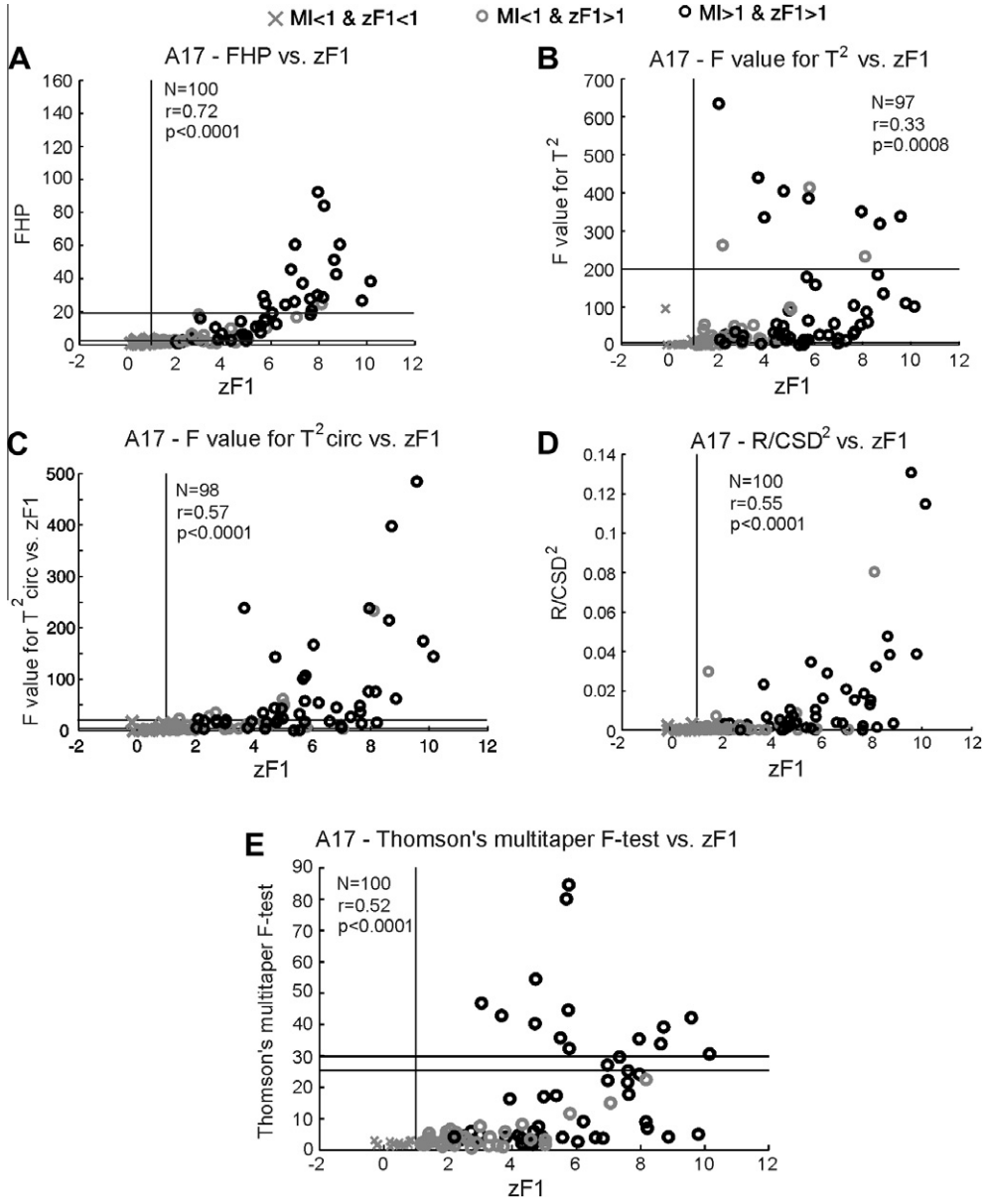

Fig. 9. Pairwise comparison of $zF1$ with F-test for hidden periodicity (FHP) (A), Hotelling T^2 statistics (B), T^2circular statistics (C), Rayleigh's phase coherence test (R/CSD^2) (D) and Thomson's multitaper F-test (E) for recordings from area 17. In all cases, bin size of PSTH which was a subject of spectral analysis, was equal to 10 ms. In all cases, apart of Thomson's multitaper F-test, *FFT* was performed to obtain amplitude and/or phase values. Thomson's multitaper F-test was calculated with Chronux toolbox with parameters of time-bandwidth set to 7 and number of tapers equal to 13. Note the best correlation between values of $zF1$ and FHP, the other index based on the comparison of response amplitude at stimulus frequency to amplitudes at other frequencies in the spectrum. The correlations of $zF1$ with other measures, although positive and significant, are weaker. Two horizontal lines in (A), (B), (C) and (E) indicate the lowest and the highest threshold for significance of F-values. All points above the upper line and non below the lower line indicate significant modulation. Significance of the RPC test (D) is calculated based on different rules (see Section 3.2). According to values of $zF1$, 87% of neurons had modulated responses, while values of FHP indicated that only 46% of neurons had such responses. T^2 and T^2_{circ} statistics respectively assessed 60% and 69% of neurons as modulated. With the use of RPC test, 57% of cells were identified as exhibiting modulations in responses. Note also, that all 5 measures in some cases resulted in low values for strongly modulated responses and high values of $zF1$.

4.4. Correlation of zF1 with MI, F1 and F0 in A17, SC, Sg and CN

In Fig. 10 we provide the pairwise comparison of *MI* and *zF*1. This comparison, reveals different patterns of distributions of values of indices and their relationships for different visual structures. For cortical and CN recordings *MI* and *zF*1 correlated well ($r = 0.564$, $p < 0.001$ and $r = 0.648$, $p < 0.001$, respectively). Weaker positive correlation was found for collicular responses ($r = 0.314$, $p = 0.01$), while in the case of Sg recordings the correlation was negative ($r = -0.225$, $p = 0.02$). Consistent with this, the proportions of SC (12%) and Sg (19%) neurons with modulated responses ($zF1 > 1$) were substantially lower than those in CN (50%) and A17 (87%). Modulated responses with low values of *MI* due to high values of *F*0 as compared to *F*1 were found mainly in A17 and Sg (Figs. 10A and D). Unmodulated responses with $MI > 1$ due to low magnitude of net responses as compared to background activity, were mostly observed for SC and CN neurons (Figs. 10B and C) and no such responses were observed in the A17 (Fig. 10A) where almost all neurons exhibit very little or no background activity (median: 0 spikes/s, mean: 1.63 spikes/s, range: 0–26.31 spikes/s; see for reviews, Gilbert, 1977; Henry, 1977).

As the value of *F*1 is crucial for assessment of modulation in analyzed spike-trains, and to provide better intuition about *zF*1 behavior, we examined correlations between *F*1 and *F*0, and *zF*1. Relationship between *F*1 and *F*0 values in all investigated structures is shown in Fig. 11. Not surprisingly, due to absence or very little spontaneous activity in A17 data, $F1 = F0$ line quite precisely divides responses with $MI > 1$ from those with $MI < 1$ (Fig. 11A). In all structures we recorded from most of the modulated responses (marked with circles in Figs. 11A–D) have higher $F1/F0$ ratios than unmodulated responses (crosses on Figs. 11A–D). However, in subcortical structures $F1 = F0$ line (or $F1/F0 = 1$ line) neither divides modulated ($zF1 > 1$) and unmodulated ($zF1 < 1$) responses, nor separates responses with $MI > 1$ from those with $MI < 1$.

In all investigated structures, *zF*1 correlated well with *F*1 value (Figs. 12A–D; A17: $r = 0.753$, $p < 0.001$; CN: $r = 0.875$, $p < 0.001$; SC: $r = 0.860$, $p < 0.001$; Sg: $r = 0.822$, $p < 0.001$).

Finally, we also tested the relationship between the values of *zF*1 and the magnitude of *F*0. The correlation between *zF*1 and *F*0 for neurons recorded from A17 was on the border of significance ($r = -0.19$, $p = 0.056$) and not significant in the case of CN ($r = -0.143$, $p = 0.15$; Figs. 12E and F) neurons. However, for both SC ($r = 0.461$, $p < 0.001$) and Sg ($r = 0.529$, $p < 0.001$) neurons the correlation was significantly positive (Figs. 12G and H, respectively).

5. Discussion

In the present paper we propose standardized *F*1, *zF*1, as a simple and intuitive tool for detection and assessment of the strength of modulations in responses of visual neurons to drifting gratings. We defined *zF*1 as the ratio of a difference between the *F*1 component of the response and the mean value of amplitude spectrum to the standard deviation of amplitude values along all frequencies in the spectrum. The *zF*1 value is easy to interpret – it detects the presence of the peak in the amplitude spectrum ($zF1 > 1$) at the temporal frequency of the grating and determines its height relative to *SD* of the spectrum.

5.1. Applicability and limitations of zF1 as a measure of strength of modulation

The *zF*1 measure is, by definition, independent of background spike activity. By contrast, in the case of *MI*, in its original form proposed by Movshon, Thompson, and Tolhurst (1978a, 1978b,

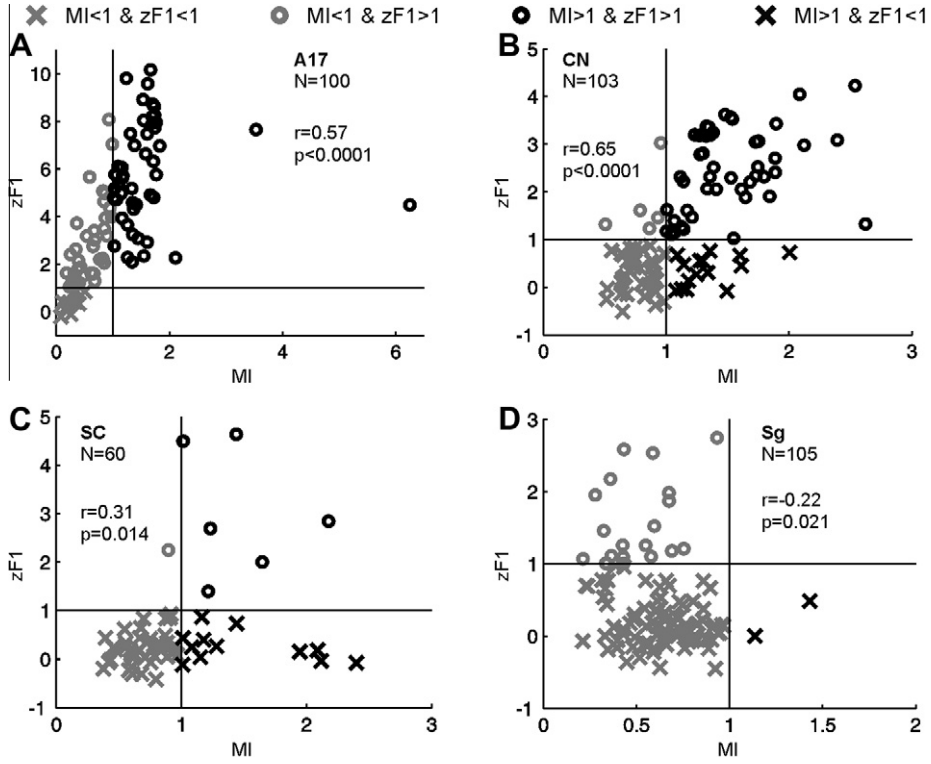

Fig. 10. Relationship between *zF*1 and *MI* for maximum net responses to optimal drifting gratings of neurons recorded from four different structures: A17 (A), CN (B), SC (C) and Sg (D). The markers are used to indicate for a particular cell whether its *MI* and *zF*1 calculated for maximal net responses were higher or lower than unity (gray: $MI < 1$, black: $MI > 1$, crosses: $zF1 < 1$, open circles: $zF1 > 1$). *N* indicates number of cells taken for the analysis. Note a good positive correlation between *zF*1 and *MI* values for A17 and CN data and low positive correlation for SC cells and low negative for Sg cells. In the case of CN, SC and Sg data, the *MI*, but not *zF*1, could take high value when no modulation was present in responses ($MI > 1$ and $zF1 < 1$).

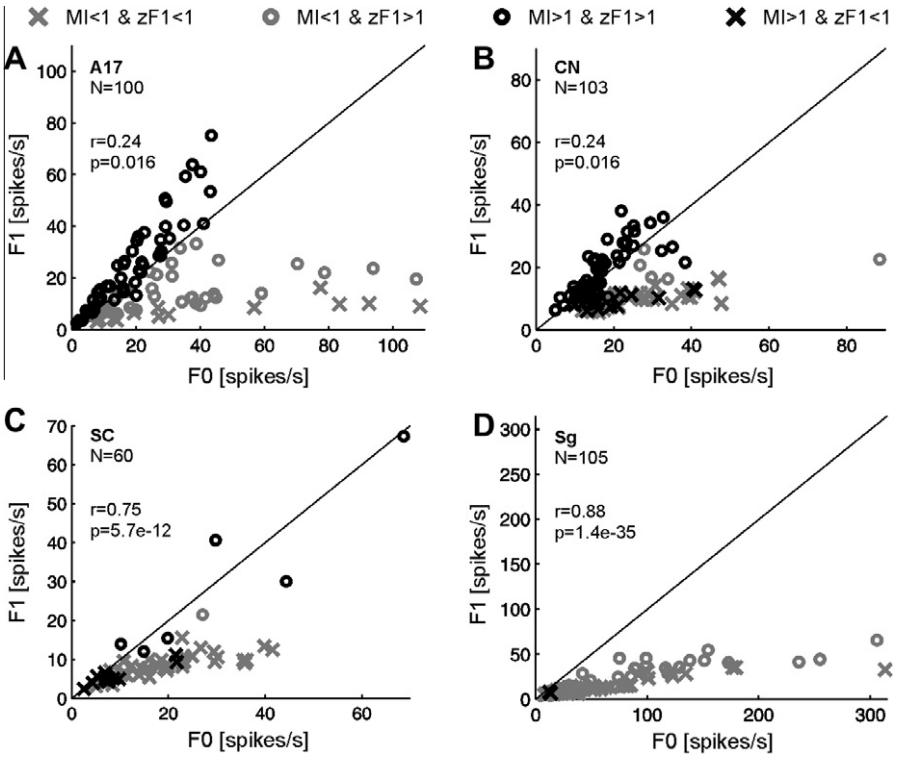

Fig. 11. Pairwise comparison of *F*1 (ordinate) vs. *F*0 (abscissa) of maximal net responses of neurons from A17 (A), CN (B), SC (C) and Sg (D) obtained for optimized stimulus parameters. For any given structure modulated responses (*zF*1 > 1) have higher *F*1/*F*0 ratio than the unmodulated responses. However, despite *MI* > 1 for some responses in Sg, SC and CN, due to the presence of some background spike activity, the *F*1/*F*0 ratio falls below unity (or the *F*1 = *F*0 line). Note the separation of low-*F*0–high-*F*1 cells from high-*F*0–low-*F*1 cells in A17.

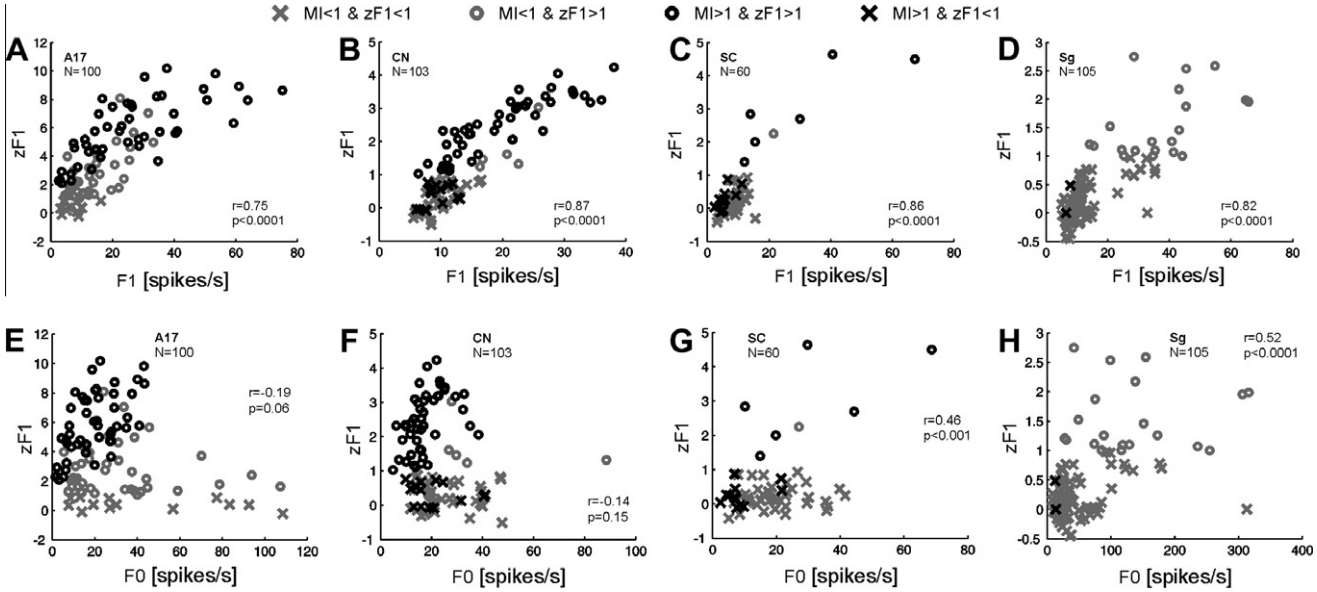

Fig. 12. Pairwise comparison of *zF*1 (ordinate) vs. *F*1 or *F*0 (abscissa) for responses of neurons from A17 (A and E), CN (B and F), SC (C and G) and Sg (D and H) obtained for optimized stimulus parameters. Note a good correlation between *zF*1 and *F*1 in all structures (A–D). On the other hand, the relationship between *zF*1 and *F*0 depends on the brain structure, from which the neurons were recorded (E–H).

Eq. (1)), relatively high background spike activity in comparison with mean firing rate increases the absolute *MI* value and may lead to a false conclusion concerning the strength of modulations. On the other hand, the *F*1/*F*0 ratio used as a modulation index will, in such situations, underestimate the strength of modulations within responses. This dependence of *MI* and *F*1/*F*0 on the background spike activity limits usefulness of the indices in studies of visual neurons exhibiting substantial background activity.

As we have demonstrated here using simulated spike-trains, the *zF*1 index is resistant to the overall spike counts. By contrast, a negative correlation between *MI* and *F*0 was found in simulated data containing both modulated component and unmodulated

component with uniform random spike distribution (present results; see also Crowder et al., 2007). For the responses of a few spikes in a second, which is quite common in the case of cortical neurons, the mean *MI* value usually exceeds unity. This in turn, would often result in identification of cells with essentially unmodulated spike-trains, as strongly phase-sensitive. The dependence of measures of the strength of oscillation in neuronal activity on firing rate is quite a common problem. Indeed, the analysis performed by Mureşan et al., (2008) comparing behavior of four measures of strength of oscillation reveals either a strong bias of the estimated values on the firing rate (secondary peak-valley difference proposed by Samonds & Bonds, 2005) or high variability, especially in the case of weak or nonexistent oscillations and low firing rate (generalized Gabor fitting; König, 1994). The oscillation score index, introduced by Mureşan et al. (2008) and defined as a ratio of the peak magnitude to averaged magnitude of the spectrum computed with *FFT* for the autocorrelation histogram of spike-train, is considered as the best of the four measures tested. However, similarly to *MI*, the oscillation score index overestimates the strength of modulations for weak or nonexistent oscillation at low firing rate (10 Hz). By contrast, as we have shown for simulated spike-trains with randomly distributed events, the *zF*1 index introduced here behaves in a predictable way and has the mean of zero and *SD* equal unity for considered response magnitudes. On the other hand, for modulated simulated data *zF*1 detects modulations almost in all data with exception of those where the amplitude of modulation is much lower than the magnitude of the unmodulated component. Thus, the index can detect oscillatory changes in temporal spiking structure both for low net response and small overall spike count. Only a weak dependance on the firing rate makes *zF*1 a valuable tool for estimation of modulation strength over a wide range of response magnitudes. The index could also be worth considering as a measure of strength of oscillation in neuronal activity not evoked by drifting grating, particularly in the case of low firing rates.

The weakness of the *zF*1 index, that lies in its assumptions, is the fact, that non-flat spectra and/or occurrences of F2 or peaks at other harmonics will influence both *mean*(*FFT*) and *SD*(*FFT*), thus also *zF*1 value itself. The presence of peaks at higher harmonics, which lead to increases of both *mean*(*FFT*) and *SD*(*FFT*), invariably leads to decrease of *zF*1. The decrease will depend on response amplitudes at higher harmonics and also on the length and resolution of the spectrum. However, in the case of non-windowed *FFT* spectra of responses to drifting gratings, both the peak at the frequency of stimulation and harmonic peaks, if present, occur at precisely defined frequencies, are very narrow, and thus, in practice, their influence on *mean*(*FFT*), *SD*(*FFT*) and *zF*1 is small. A possible solution to deal with the problem of non-flat spectra would be to substitute *mean*(*FFT*) and *SD*(*FFT*) computed for the whole spectrum by *mean* and *SD* computed from reasonable surrounding of main frequency of interest, similarly as proposed by Mureşan et al. (2008) for assessment of oscillation score.

In agreement with theoretical predictions, we showed that values of both *MI* and *zF*1 indices can depend on the length of PSTH (or duration of recorded spike-train). Although the *MI* value for unmodulated simulated data increases for shorter recordings (Fig. 7A), in the case of modulations in responses of cortical neurons, the index is relatively resistant to the length of the recording epoch (Fig. 5D). Behavior of *zF*1 is the opposite – for unmodulated data the index is not sensitive to PSTH length but its value increases for longer modulated spike-trains. If longer epochs are used, the *zF*1 index appears to be more able to 'detect' weak modulations. In general, dependence of both indices on the length of the recording epoch is a disadvantage, and the longer spike-trains the better.

Another weakness of the *zF*1 index is dependence of its value on bin size of PSTH (Fig. 4D and E). In this respect, the recording and data analysis with high temporal resolution is preferable. The observed difference of the values of the index between 10 ms and 1 ms bin size, however, virtually did not affect the classification of neuronal responses as modulated ($zF1 > 1$) or unmodulated ($zF1 < 1$).

More generally, the *zF*1 value is dependent on the number of frequencies in the spectrum (due to the duration of spike-train, or due to the bin size of analyzed PSTH). This dependence is caused by the fact that spectral energy density remains unchanged in the case of different signal lengths or temporal resolution (Eq. (2)). Thus, the mean value of the spectrum (so also the *F*1 value in the case of unmodulated spike-trains) is reduced for a set of data collected over longer epochs or with higher resolutions. On the other hand, for stationary modulated data *F*1 is independent of the length of recording because part of the energy is strictly accumulated at certain temporal frequency. Thus in practice the *F*1 is independent of the number of frequencies in the spectrum. Overall, it appears that at least for one sort of data, modulated or unmodulated, any index derived from *FFT* would depend on the duration of recording epoch or temporal resolution of the data. Proposed here normalization of *zF*1 allows one to overcome this problem and recalculate *zF*1 values obtained from spectra of different ranges and/or resolutions. However, taking into account distortion introduced by large bin size (Figs. 4D and 6A) we recommend the use of as small as possible bin sizes in PSTHs, from which frequency spectra are computed (see also Gabbiani & Koch, 1998).

Despite the aforementioned weaknesses, the advantages discussed above, make *zF*1 suitable measure to detect the temporal frequency modulation and assess their strength in responses of visually active neurons recorded from both cortical and subcortical visual structures of the mammalian brain.

5.2. Comparison with other methods

In the present study we compared *zF*1 values obtained with the use of conventional *FFT* to the values obtained using Welch's approach and multitaper method. The *zF*1 values correlated well, although the correlation was lower for Welch method. In both cases the *zF*1 values tended to be lower than those obtained with conventional *FFT* (Fig. 8). Both Welch's and multitaper approaches result in smoother spectra than those obtained with *FFT*, but they lead to broadening of modulation peaks. This in turn, affects standard deviations of the spectra and leads to lowering of *zF*1 values, and thus decreasing the sensitivity of the index. In the case of both methods the exact shape of obtained spectra (including height and the broadness of possible modulation peaks) depend on the more or less arbitrarily set parameters. The problem of choosing proper parameters makes those methods not very useful in the case of automated analysis. Therefore, we suggest the use of standard *FFT* to obtain the spectrum.

To identify and assess strength of modulations in the responses by the stimulus in the form of luminance-modulated sine-wave moving gratings we used five different measures representing different approaches. Consistency in phase of Fourier function component at stimulus frequency was assessed by Rayleigh's Phase Coherence test (RPC, Mardia, 1972; Picton et al., 1987; Ahmar, Wang, & Simon, 2005). We used two tests which take into account both phase and amplitude values of response: Hotelling T^2 test (Picton et al., 1987, 2001) and T^2 circular statistics (Victor & Mast, 1991). Finally, we used the *F*-test for hidden periodicity (FHP, Picton et al., 2001; Ahmar, Wang, & Simon, 2005) and Thomson's multitaper *F*-test (Mitra & Pesaran, 1999; Thomson, 1982), which are based on the comparison of magnitude of amplitude component in the frequency spectra at frequency of stimulation, *F*1, to measurements at other frequencies in the spectra. Using cortical data, we have compared *zF*1 with other methods of assessment of

strength of modulations (Fig. 9). In all the cases correlation was positive and significant ($0.33 \leqslant r \leqslant 0.72$, $p < 0.001$). *zF*1 allowed to identify 87% of neurons as having modulated responses, while other methods assessed percentage of significantly modulated neurons between 15% (in the case of Thomson's multitaper *F*-test) and 69% (in the case of T^2 circular statistics) and in some cases failed to detect clear modulation, even when value of *zF*1 was very high. This, together with high efficacy of detection of modulations in the case of simulated modulated data, implies higher sensitivity of *zF*1 in comparison to other methods.

Another problem is the limited applicability of methods which exploit phase at stimulus frequency (Rayleigh's Phase Coherence test, Hotelling T^2 test and T^2 circular statistics). These measures may be used only in the case of presentation of sinusoidal gratings with constant phase across trials and can be assessed only using conventional *FFT*, but they cannot be applied to spectra obtained with Welch's or multitaper approaches. In this respect, the methods based on comparison of the magnitude of the amplitude component at the frequency of stimulation to measurements at other frequencies in the spectra (*F*-test for hidden periodicity, Thomson's multitaper *F*-test and *zF*1) are more universal.

However, thinking of broader applications of *zF*1, and in order to deeper understand its behavior, one should conduct additional tests and comparisons of *zF*1 with the above listed methods using a wider range of physiological and simulated data which include bursting activities, internal oscillations, nonlinearities, different types of noise, etc. Further studies are warranted to address these issues.

5.3. Comparison of temporal frequency modulation of neuronal responses in SC, SG, CN and primary visual cortex

Using *zF*1 we have compared the temporal frequency modulation of visual responses of neurons recorded in four brain structures. While responses of neurons in the primary visual cortex or CN were often strongly modulated by the temporal frequency of the stimulation, strong temporal frequency modulation of responses of Sg and SC neurons was not common. Indeed, in both A17 and CN, responses were deeply modulated by drifting gratings and *zF*1 correlated well with the *MI* and *F*1 values, but not with *F*0 values. By contrast, there was only a weak correlation between *zF*1 and *MI* indices in case of responses of Sg and SC neurons, while the correlation between *zF*1 and *F*0 for these structures was relatively strong.

The strengths of temporal modulations of responses of CN neurons was much greater than those of Sg and SC neurons. In view of remarkable similarity of many characteristics of responses of Sg, SC and CN neurons (Nagy et al., 2008; Paróczy et al., 2006; Waleszczyk et al., 2007) we are surprised by the dissimilarity in the strength of temporal frequency response modulation of Sg and SC neurons vs. that of CN neurons. Thus, the question arises what underlies strong temporal frequency modulation in the CN. Earlier morphological findings in eutherian carnivores (cats) and lagomorphs (rabbits) stressed the predominant role of the geniculostriate pathway in conveying visual information to the CN (Hollander, Tietze, & Distel, 1979; Webster, 1965), while recent morphological and physiological studies support the suggestion that the extrageniculate ascending tectofugal pathways in mammals also project to the CN (Guirado, Real, & Davila, 2005; Harting, Updyke, & Van Lieshout, 2001a; Harting, Updyke, & Van Lieshout, 2001b; Hoshino et al., 2009). One possibility is that the inputs from the primary visual cortex and/or the anterior ectosylvian cortex, may underpin the temporal frequency modulation in the CN (Nagy et al., 2011). It is worth noting in the context that despite the fact that the dorsolateral part of CN, unlike A17, does not receive direct input from the dorsal lateral geniculate nucleus (see Harting, Updyke, & Van Lieshout, 2001a cf. also Nagy et al., 2003, 2008), the great majority of CN exhibits *MI* and *zF*1 indices characteristic of the simple rather than complex cells in A17.

5.4. Usefulness of the zF1 for the simple/complex classification

The existence of the simple/complex dichotomy, rather than the continuum, and its relation to cortical circuitry remains controversial (Abbott & Chance, 2002; Chance, Nelson, & Abbott, 1999; Mechler & Ringach, 2002; Priebe et al., 2004). Recent studies, however, showing a correlation between laminar location and spatial phase-sensitivity of cortical neurons support the idea that the simple/complex division has functional significance (Martinez et al., 2005; Williams & Shapley, 2007).

Cortical cells are identified as simple if $MI > 1$ or as complex if $MI < 1$ (De Valois, Albrecht, & Thorell, 1982; see for review Skottun et al., 1991). It is commonly reported that frequency histogram of *MI* values obtained for neurons recorded from primary visual cortices has non-unimodal distribution (see Ibbotson, Price, & Crowder, 2005; Romo et al., 2011; Skottun et al., 1991; cf. however: Bardy et al., 2006; Dean & Tolhurst, 1983). Skottun and his colleagues (1991) argued that *MI* values of the large sample of cat and macaque monkey area 17 neurons recorded in six different laboratories, fell into bimodal distributions with peaks at *MI* values of 1.7 for simple cells and 0.2 (cat)–0.3 (monkey) for complex cells and a clear minimum or dip in histograms for *MI* value close to unity. Similarly, Ibbotson and colleagues (2005) analyzing simple and complex cells recorded from area 17 of marsupial, Tammar wallaby (*Macropus eugenii*), reported non-unimodal distribution in frequency histogram of *MI* with peaks at 1.5 for simple and 0.3 for complex cells and with the division line close to unity.

The question arises whether measuring *zF*1 presents any value for proper subdivision of neurons in primary visual cortices into simple and complex classes. *zF*1 seems to be a good tool for detection of modulation ($zF1 > 1$) in the whole range of response magnitudes. Overall, identification of cells as simple or complex, is not based on the presence vs. complete absence of modulations in responses to drifting gratings. Indeed, complex cells are 'allowed' to exhibit some degree of modulations. On the other hand, the cell should not be identified as simple if it does not exhibit at least some degree of spatial phase modulations in responses to grating. At low firing rate, computation of *MI* in parallel with *zF*1 creates opportunity to minimize the number of false positive identifications of cells as simple.

It is commonly accepted that the *MI* index (or *F*1/*F*0 ratio in the case of virtually no background spike activity) is a measure of linearity of spatial summation in the neuron's receptive field (Movshon, Thompson, & Tolhurst, 1978a, 1978b; Skottun et al., 1991). With a qualitative approach, the identification of cells as simple or complex is based on the existence (simple) or lack (complex) of spatially separate ON and OFF discharge subregions in their receptive fields. It has been shown that when the *MI* index is used, there is a good correspondence between the two methods of identification (Bardy et al., 2006; Cardin, Palmer, & Contreras, 2008; Dean & Tolhurst, 1983; Mata & Ringach, 2005; Priebe et al., 2004; Skottun et al., 1991; see however, Kagan, Gur, & Snodderly, 2002). Degree of separation (or overlap) of ON and OFF discharge subregions can be estimated using various measures (Mata & Ringach, 2005). Lack of adequate data, however, did not allow us to examine the relationship between those measures and *zF*1 index. A degree of correlation of *zF*1 index with measures of separation/overlap of ON and OFF discharge subregions in the receptive fields of neurons and with the push–pull index proven to be a useful tool in simple/complex classification (Martinez et al., 2005) can be a subject of further studies.

5.5. Some future directions

It is postulated that in the visual system at least, signal transmission is more effective in the bursting rather than tonic mode of neuronal activity (Kara & Reid, 2003; Rathbun, Warland, & Usrey, 2010; Usrey, Alonso, & Reid, 2000; see for review Sherman, 2005). Similarly, modulations in neuronal responses to gratings could lead to more effective signal transmission to the postsynaptic neuron by temporal summation of the bursting-like, phase-sensitive input. This would suggest advantage of simple over complex cells in effectiveness and reliability of signal transmission. Indeed, Mechler and his colleagues (Mechler, Reich, & Victor, 2002) concluded that simple cells in macaque A17 are more effective in feature discrimination and carry twice as much of feature information than complex cells. Higher spatial phase-sensitivity of primary visual cortex neurons responding to drifting gratings has been reported for: (1) non-dominant eye (vs. dominant; Skottun & Freeman, 1984); (2) reversible inactivation of feedback input from higher cortical area (Bardy et al., 2006); (3) co-activation of the center and silent suppressive surround of receptive field (Bardy et al., 2006; Romo et al., 2011) and (4) low contrast stimulation (Crowder et al., 2007; van Kleef, Cloherty, & Ibbotson, 2010). Invariably, in all the above cases an increase of the spatial phase-sensitivity corresponded to decrease in the firing rate. One can argue that in the case of non-optimal, low-firing-rate-generating stimuli, it would be a 'wise solution' for cortical circuit to switch into a 'simple' modulated mode of response to ensure the reliability of signal transmission. On the other hand, in the present study we show that in simulated, modulated and unmodulated data there is a negative correlation between the value of *MI* and firing rate. Thus, the 'simplification' of responses especially at the very low firing rates as assessed by the *MI* might be more apparent than real. Further studies are needed to resolve this issue. The *zF*1, being reliable at low firing rate, seems to be a proper tool for this purpose.

In conclusion, the *zF*1 appears to constitute a suitable tool for reliable assessment of the strength of modulation of neuronal activity. The index is particularly useful for assessment of the strength of modulation when firing rates and/or net mean responses are low.

Acknowledgments

We would like to thank Drs. Cedric Bardy, Thomas FitzGibbon and Jin Yu Huang for their participation in recordings from area 17 and Drs. Zuzanna Paróczy, Zita Márkus, Antal Berényi and Gabriella Eördegh for their participation in recordings from subcortical structures. We would also like to thank the Reviewers for their valuable suggestions to improvement the quality of the paper.

The work was supported by grants from Australian Research Council Centre of Excellence in Vision Science and the National Health and Medical Research Council of Australia, Polish Ministry of Science and Higher Education Grant N N303 070234 and National Science Center Grant N N303 820640, OTKA/Hungary Grants: 68594, 75156.

Appendix A. Normalization concerning number of frequencies in the spectrum

The *zF*1 value, as defined in Eq. (1) (Section 3.1), is dependent on the duration of the recording and bin size of peristimulus time histogram (PSTH) used for computation of Fourier spectra. Duration of the recording determines frequency resolution of the Fourier spectrum while temporal resolution of PSTH (bin size) determines frequency range of the obtained spectrum. In general both factors determine number of frequencies in the resulting frequency spectrum.

The question thus arises how to normalize the *zF*1 value so that it can be directly compared with *zF*1 values computed from spectra containing given number of frequencies.

Assume that $\boldsymbol{x}$ and $\boldsymbol{y}$ are signals generated in the same process, however due to differences in sampling frequency and/or signal duration $\boldsymbol{y}$ is N times longer than $\boldsymbol{x}$ ($N > 0$). Let X_i and Y_j be the amplitudes of Fourier spectra $FFT(\boldsymbol{x})$ and $FFT(\boldsymbol{y})$, respectively. We also need to ensure that the Fourier spectra are properly normalized – so that the values in the amplitude spectra reflect the actual amplitudes of the components of the signal.

According to Parseval's Theorem the total powers of the spectra are equal:

$$\Sigma(X_i^2) = \Sigma(Y_j^2).$$

As the number of frequencies in $FFT(\boldsymbol{y})$ is N times higher than in $FFT(\boldsymbol{x})$, we can conclude that

$mean(Y^2) = mean(X^2)/N$.

Assuming that the signals consist of white noise and their spectra are flat we may take:

$$mean(X^2) = [mean(X)]^2$$

and conclude that:

$$mean(Y) = mean(X)/\sqrt{N}, \tag{A.1}$$

which means that mean value of the spectrum of N times longer signal is $\sqrt{N}$ times lower.

The same applies to standard deviation (SD):

$$SD(Y) = SD(X)/\sqrt{N}. \tag{A.2}$$

If signals $\boldsymbol{x}$ and $\boldsymbol{y}$ are identically modulated, and since energy of modulation is precisely accumulated in the frequency of modulation, the $F1$ values would not be affected by the lengths of the recordings or by the bin sizes of PSTHs. Therefore, $F1$s obtained from $\boldsymbol{x}$ and $\boldsymbol{y}$ should be equal.

Taking into account (A.1) and (A.2) we get:

$$zF1(y) = [F1 - mean(Y)]/SD(Y) = [F1 - mean(X)/\sqrt{N}]/[SD(x)/\sqrt{N}],$$

hence

$$zF1(y) = [F1 \cdot \sqrt{N} - mean(X)]/SD(X).$$

Thus, computation of *zF*1 from spectra with N times higher number of frequencies (Y), results in the value, that would be obtained for shorter spectrum (X) in which amplitude at the stimulus frequency would be equal $F1$ multiplied by $\sqrt{N}$. Therefore, in order to normalize the value computing the index for longer spectrum, one should divide $F1$ by $\sqrt{N}$:

$$zF1_{norm}(y) = [F1/\sqrt{N} - mean(Y)]/SD(Y).$$

For example, to normalize the *zF*1 index to 1 s length, one should divide $F1$ by $\sqrt{N}$, where N is length of recording in seconds. And to normalize the *zF*1 to desired sampling frequency one should divide $F1$ by square root of ratio of sampling frequency of the analyzed signal and the sampling frequency of interest.

If the signals are not modulated ($F1 \approx \text{mean}(X)$ and $zF1 \approx 0$) the normalization will result in further lowering of the value of *zF*1 and thus will not lead to false detection of modulations.

The assumptions which have been made, in general do not have to be fulfilled and the above formula acts as an approximation. However, as indicated in Fig. 5B in practice the approximation provides good results.

Appendix B. Estimation of the upper limit of *zF*1

To estimate the upper limit of *zF*1 we consider a purely sinusoidal signal. The ideal amplitude spectrum of such a signal will be equal to 0 everywhere, with the exception of the modulation frequency, where the value will be equal to *F*1.

Let N be the length of the amplitude spectrum.

Thus

$$mean(FFT) = F1/N \tag{B.1}$$

and

$$SD(FFT) = \sqrt{\{\Sigma[X_i - mean(FFT)]^2/(N-1)\}},$$

where X_i are the amplitude values of the spectrum.

In the considered case $N-1$ values in the spectrum are equal to 0, and one value is equal to *F*1, thus

$$SD(FFT) = \sqrt{\{[(N-1)(0-mean(FFT))^2 + (F1-mean(FFT))^2]/(N-1)\}}.$$

Using (B.1) we get:

$$SD(FFT) = \sqrt{\{[(N-1)(F1/N)^2 + (F1-F1/N)^2]/(N-1)\}}.$$

A few simple transformations lead to:

$$SD(FFT) = F1\sqrt{N}/N. \tag{B.2}$$

Putting (B.1) and (B.2) into the *zF*1 formula:

$$zF1 = (F1 - mean(FFT))/SD(FFT),$$

we obtain

$$zF1 = (F1 - F1/N)/(F1\sqrt{N}/N).$$

Simple reduction results in:

$$zF1 = (N-1)/\sqrt{N}.$$

The estimation of the upper limit of *zF*1 for a purely sinusoidal signal is shown in Fig. 5C.

References

Abbott, L. F., & Chance, F. S. (2002). Rethinking the taxonomy of visual neurons. *Nature Neuroscience, 5*, 391–392.

Ahmar, N. E., Wang, Y., & Simon, J. Z. (2005). Significance tests for MEG response detection. In *Proceedings of the 2nd international IEEE EMBS* (pp. 5–8).

Anderson, T. W. (2003). *An introduction to multivariate statistical analysis* (third ed.). New York: Wiley.

Bach, M., & Meigen, T. (1999). Do's and don'ts in Fourier analysis of steady-state potentials. *Documenta Ophthalmologica, 99*, 69–82.

Bardy, C., Huang, J. Y., Wang, C., FitzGibbon, T., & Dreher, B. (2006). 'Simplification' of responses of complex cells in cat striate cortex: Suppressive surrounds and 'feedback' inactivation. *Journal of Physiology, 574*, 731–750.

Barlow, H. B., Blakemore, C., & Pettigrew, J. D. (1967). The neural mechanism of binocular depth discrimination. *Journal of Physiology, 193*, 327–342.

Bishop, P. O., Kozak, W., & Vakkur, G. J. (1962). Some quantitative aspects of the cat's eye: Axis and plane of reference, visual field coordinates and optics. *Journal of Physiology, 163*, 466–502.

Burke, W., Dreher, B., Michalski, A., Cleland, B. G., & Rowe, M. H. (1992). The effects of selective pressure block of Y-type optic nerve fibers on the receptive field properties of neurons in the striate cortex of the cat. *Visual Neuroscience, 9*, 47–64.

Carandini, M., & Ferster, D. (2000). Membrane potential and firing rate in cat primary visual cortex. *Journal of Neuroscience, 20*, 470–484.

Cardin, J. A., Palmer, L. A., & Contreras, D. (2008). Cellular mechanisms underlying stimulus-dependent gain modulation in primary visual cortex neurons *in vivo*. *Neuron, 59*, 150–160.

Casanova, C., Freeman, R. D., & Nordmann, J. P. (1989). Monocular and binocular response properties of cells in the striate-recipient zone of the cat's lateral posterior–pulvinar complex. *Journal of Neurophysiology, 62*, 544–557.

Chance, F. S., Nelson, S. B., & Abbott, L. F. (1999). Complex cells as cortically amplified simple cells. *Nature Neuroscience, 2*, 277–282.

Crowder, N. A., van Kleef, J., Dreher, B., & Ibbotson, M. R. (2007). Complex cells increase their phase sensitivity at low contrasts and following adaptation. *Journal of Neurophysiology, 98*, 1155–1166.

De Valois, R. L., Albrecht, D. G., & Thorell, L. G. (1982). Spatial frequency selectivity of cells in macaque visual cortex. *Vision Research, 22*, 545–559.

Dean, A. F., & Tolhurst, D. J. (1983). On the distinctness of simple and complex cells in the visual cortex of the cat. *Journal of Physiology, 344*, 305–325.

Fisher, R. A. (1929). Tests of significance in harmonic analysis. *Proceedings of Royal Society of London Ser A, 125*, 54–59.

Gabbiani, F., & Koch, C. (1998). Principles of spike train analysis. In Koch, C., & Segev, I. (Eds.), *Methods in neuronal modelling* (pp. 313–360). MIT Press.

Gilbert, C. D. (1977). Laminar differences in receptive field properties of cells in cat primary visual cortex. *Journal of Physiology, 268*, 39–421.

Guirado, S., Real, M. A., & Davila, J. C. (2005). The ascending tectofugal visual system in amniotes: New insights. *Brain Research Bulletin, 66*, 290–296.

Harting, J. K., Updyke, B. V., & Van Lieshout, D. P. (2001a). Striatal projections from the cat visual thalamus. *European Journal of Neuroscience, 14*, 893–896.

Harting, J. K., Updyke, B. V., & Van Lieshout, D. P. (2001b). The visual-oculomotor striatum of the cat: Functional relationship to the superior colliculus. *Experimental Brain Research, 136*, 138–142.

Henry, G. H. (1977). Receptive field classes of cells in the striate cortex of the cat. *Brain Research, 133*, 1–28.

Hicks, T. P., Benedek, G., & Thurlow, G. A. (1988). Organization and properties of neurons in a visual area within the insular cortex of the cat. *Journal of Neurophysiology, 60*, 397–421.

Hollander, H., Tietze, J., & Distel, H. (1979). An autoradiographic study of the subcortical projections of the rabbit striate cortex in the adult and during postnatal development. *Journal of Comperative Neurology, 184*, 783–794.

Hoshino, K., Eördegh, G., Nagy, A., Benedek, G., & Norita, M. (2009). Overlap of nigrothalamic terminals and thalamostriatal neurons in the feline lateralis medialis-suprageniculate nucleus. *Acta Physiologica Hungarica, 96*, 203–211.

Hotelling, H. (1931). The generalization of Students's ratio. *The Annals of Mathematical Statistics, 2*, 360–378.

Hubel, D. H., & Wiesel, T. N. (1959). Receptive fields of single neurons in the cat's striate cortex. *Journal of Physiology, 148*, 574–591.

Hubel, D. H., & Wiesel, T. N. (1962). Receptive fields, binocular interaction and functional architecture in the cat's visual cortex. *Journal of Physiology, 160*, 106–154.

Ibbotson, M. R., Price, N. S., & Crowder, N. A. (2005). On the division of cortical cells into simple and complex types: A comparative viewpoint. *Journal of Neurophysiology, 93*, 3699–3702.

Kagan, I., Gur, M., & Snodderly, D. M. (2002). Spatial organization of receptive fields of V1 neurons of alert monkeys: Comparison with responses to gratings. *Journal of Neurophysiology, 88*, 2557–2574.

Kara, P., & Reid, R. C. (2003). Efficacy of retinal spikes in driving cortical responses. *Journal of Neuroscience, 23*, 8547–8557.

König, P. (1994). A method for the quantification of synchrony and oscillatory properties of neuronal activity. *Journal of Neuroscience Methods, 54*, 31–37.

Mardia, K. V. (1972). *Statistics of directional data* (p. 357). Academic Press, New York.

Martinez, L. M., Wang, Q., Reid, R. C., Pillai, C., Alonso, J. M., Sommer, F. T., & Hirsch, J. A. (2005). Receptive field structure varies with layer in the primary visual cortex. *Nature Neuroscience, 8*, 372–379.

Mata, M. L., & Ringach, D. L. (2005). Spatial overlap of ON and OFF subregions and its relation to response modulation ratio in macaque primary visual cortex. *Journal of Neurophysiology, 93*, 919–928.

Mechler, F., Reich, D. S., & Victor, J. D. (2002). Detection and discrimination of relative spatial phase by V1 neurons. *Journal of Neuroscience, 22*, 6129–6157.

Mechler, F., & Ringach, D. L. (2002). On the classification of simple and complex cells. *Vision Research, 42*, 1017–1033.

Mitra, P. P., & Pesaran, B. (1999). Analysis of dynamic brain imaging data. *Biophysical Journal, 76*, 691–708.

Movshon, J. A., Thompson, I. D., & Tolhurst, D. J. (1978a). Spatial summation in the receptive fields of of simple cells in the cat's striate cortex. *Journal of Physiology, 283*, 53–77.

Movshon, J. A., Thompson, I. D., & Tolhurst, D. J. (1978b). Receptive field organization of complex cells in the cat's striate cortex. *Journal of Physiology, 283*, 79–99.

Mureşan, R. C., Jurjuţ, O. F., Moca, V. V., Singer, W., & Nikolić, D. (2008). The oscillation score: An efficient method for estimating oscillation strength in neuronal activity. *Journal of Neurophysiology, 99*, 1333–1353.

Nagy, A. J., Berényi, A., Gulya, K., Norita, M., Benedek, G., & Nagy, A. (2011). Direct projection from the visual associative cortex to the caudate nucleus in the feline brain. *Neuroscience Letters, 503*, 52–57.

Nagy, A., Eördegh, G., Norita, M., & Benedek, G. (2003). Vsual receptive field properties of neurons in the feline caudate nucleus. *European Journal of Neuroscience, 18*, 449–452.

Nagy, A., Paróczy, Z., Márkus, Z., Berényi, A., Wypych, M., Waleszczyk, W. J., & Benedek, G. (2008). Drifting grating stimulation reveals particular activation properties of visual neurons in the caudate nucleus. *European Journal of Neuroscience, 27*, 1801–1808.

Paróczy, Z., Nagy, A., Márkus, Z., Waleszczyk, W. J., Wypych, M., & Benedek, G. (2006). Spatial and temporal visual properties of single neurons in the suprageniculate nucleus of the thalamus. *Neuroscience, 137*, 1397–1404.

Picton, T. W., Dimitrijevic, A., John, M. S., & Van Roon, P. (2001). The use of phase in the detection of auditory steady-state responses. *Clinical Neurophysiology, 112*, 1698–1711.

Picton, T. W., Vajsar, J., Rodriguez, R., & Campbell, K. B. (1987). Reliability estimates for steady-state evoked potentials. *Electroencephalography & Clinical Neurophysiology, 68*, 119–131.

Priebe, N. J., Mechler, F., Carandini, M., & Ferster, D. (2004). The contribution of spike threshold to the dichotomy of cortical simple and complex cells. *Nature Neuroscience, 7*, 1113–1122.

Purpura, K. P., & Bokil, H. (2008). *Neural signal processing: Tutorial 1* (pp. 67–77). <http://www.sfn.org/siteobjects/published/0000BDF20016F63800FD712C30FA42DD/3C7DD4CD67C8FFD21EF726E0AA9AD416/file/8%20Purpura%20Short%20Course%20Syllabus.pdf>.

Rathbun, D. L., Warland, D. K., & Usrey, W. M. (2010). Spike timing and information transmission at retinogeniculate synapses. *Journal of Neuroscience, 30*, 13558–13566.

Rodieck, R. W., Pettigrew, J. D., Bishop, P. O., & Nikara, T. (1967). Residual eye movements in receptive-field studies of paralyzed cats. *Vision Research, 7*, 107–110.

Romo, P. A., Wang, C., Zeater, N., Solomon, S. G., & Dreher, B. (2011). Phase sensitivities, excitatory summation fields, and silent suppressive receptive fields of single neurons in the parastriate cortex of the cat. *Journal of Neurophysiology, 106*, 1688–1722.

Samonds, J. M., & Bonds, A. B. (2005). Gamma oscillation maintains stimulus structure-dependent synchronization in cat visual cortex. *Journal of Neurophysiology, 93*, 223–236.

Sanderson, K. J., & Sherman, S. M. (1971). Nasotemporal overlap in visual field projected to lateral geniculate nucleus in the cat. *Journal of Neurophysiology, 34*, 453–466.

Schuster, A. (1898). On the investigation of hidden periodicities with application to a supposed 26 day period of meteorological phenomena. *Terrestrial Magnetism and Atmospheric Electricity, 3*, 13–41.

Sherman, S. M. (2005). Thalamic relays and cortical functioning. *Progress in Brain Research, 149*, 107–126.

Siegel, S. (1956). *Nonparametric statistics for the behavioral sciences: International student edition*. Tokyo: McGraw-Hill Kogakusha Ltd., p. 40.

Skottun, B. C., De Valois, R. L., Grosof, D. H., Movshon, J. A., Albrecht, D. G., & Bonds, A. B. (1991). Classifying simple and complex cells on the basis of response modulation. *Vision Research, 31*, 1079–1086.

Skottun, B. C., & Freeman, R. D. (1984). Stimulus specificity of binocular cells in the cat's visual cortex: Ocular dominance and the matching of left and right eyes. *Experimental Brain Research, 56*, 206–216.

Thomson, D. J. (1982). Spectrum estimation and harmonic analysis. *Proceedings of the IEEE, 70*, 1055–1096.

Usrey, W. M., Alonso, J. M., & Reid, R. C. (2000). Synaptic interactions between thalamic inputs to simple cells in cat visual cortex. *Journal of Neuroscience, 20*, 5461–5467.

van Kleef, J. P., Cloherty, S. L., & Ibbotson, M. R. (2010). Complex cell receptive fields: Evidence for a hierarchical mechanism. *Journal of Physiology, 588*, 3457–3470.

Victor, J. D., & Mast, J. (1991). A new statistic for steady-state evoked potentials. *Electroencephalography & Clinical Neurophysiology, 78*, 378–388.

Waleszczyk, W. J., Nagy, A., Wypych, M., Berenyi, A., Paróczy, Z., Eordegh, G., Ghazaryan, A., & Benedek, G. (2007). Spectral receptive field properties of neurons in the feline superior colliculus. *Experimental Brain Research, 181*, 87–98.

Webster, K. E. (1965). The cortico-striatal projections in the cat. *Journal of Anatomy, 99*, 329–337.

Williams, P. E., & Shapley, R. M. (2007). A dynamic nonlinearity and spatial phase specificity in macaque V1 neurons. *Journal of Neuroscience, 27*, 5706–5718.

Wypych, M., Nagy, A., Paróczy, Z., Márkus, Z., Berényi, A., Benedek, G., et al. (2009a). A new method for identification of modulation in neural responses to drifting grating stimulation. *Acta Neurobiologiae Experimentalis (Wars)*, 69, 324.

Wypych, M., Nagy, A., Paróczy, Z., Márkus, Z., Berényi, A., Benedek, G., et al. (2009b). Temporal frequency modulation of neuronal activity in the supragenicular nucleus of the posterior thalamus. In *41st EBBS congress*, 13–18.09.2009, Rhodes, Greece.

Wypych, M., Wang, C., Dreher, B., & Waleszczyk, W. J. (2010). A new method of assessment of strength of modulations in the responses of single visual neurons to drifting achromatic sine-wave gratings: Comparison with evaluations based on classical modulation index. *FENS Abstract, 5*, 081.39.

Zar, J. H. (1999). *Biostatistical analysis* (fourth ed.). Upper Saddle River, NJ: Prentice-Hall.